Icarus 302 (2018) 386–406

Contents lists available at ScienceDirect

Icarus

journal homepage: www.elsevier.com/locate/icarus

Clastic polygonal networks around Lyot crater, Mars: Possible formation mechanisms from morphometric analysis

L.M. Brooker[a,*], M.R. Balme[a], S.J. Conway[b], A. Hagermann[a], A.M. Barrett[a], G.S. Collins[c], R.J. Soare[d]

[a] Department of Physical Sciences, Open University, Walton Hall, Milton Keynes MK7 6AA, UK
[b] CNRS Laboratoire de Planétologie et Géodynamique de Nantes, Université de Nantes, 2 rue de la Houssiniére, 44322 Nantes, France
[c] Department of Earth Science and Engineering, Imperial College, Kensington, London SW7 2BP, UK
[d] Department of Geography, Dawson College, Montreal H3Z 1A4, Canada

ARTICLE INFO

Article history:
Received 6 March 2017
Revised 9 October 2017
Accepted 20 November 2017
Available online 21 November 2017

Keywords:
Mars, surface
Mars, climate
Geological processes

ABSTRACT

Polygonal networks of patterned ground are a common feature in cold-climate environments. They can form through the thermal contraction of ice-cemented sediment (i.e. formed from fractures), or the freezing and thawing of ground ice (i.e. formed by patterns of clasts, or ground deformation). The characteristics of these landforms provide information about environmental conditions. Analogous polygonal forms have been observed on Mars leading to inferences about environmental conditions. We have identified clastic polygonal features located around Lyot crater, Mars (50°N, 30°E). These polygons are unusually large (>100 m diameter) compared to terrestrial clastic polygons, and contain very large clasts, some of which are up to 15 metres in diameter. The polygons are distributed in a wide arc around the eastern side of Lyot crater, at a consistent distance from the crater rim. Using high-resolution imaging data, we digitised these features to extract morphological information. These data are compared to existing terrestrial and Martian polygon data to look for similarities and differences and to inform hypotheses concerning possible formation mechanisms. Our results show the clastic polygons do not have any morphometric features that indicate they are similar to terrestrial sorted, clastic polygons formed by freeze-thaw processes. They are too large, do not show the expected variation in form with slope, and have clasts that do not scale in size with polygon diameter. However, the clastic networks are similar in network morphology to thermal contraction cracks, and there is a potential direct Martian analogue in a sub-type of thermal contraction polygons located in Utopia Planitia. Based upon our observations, we reject the hypothesis that polygons located around Lyot formed as freeze-thaw polygons and instead an alternative mechanism is put forward: they result from the infilling of earlier thermal contraction cracks by wind-blown material, which then became compressed and/or cemented resulting in a resistant fill. Erosion then leads to preservation of these polygons in positive relief, while later weathering results in the fracturing of the fill material to form angular clasts. These results suggest that there was an extensive area of ice-rich terrain, the extent of which is linked to ejecta from Lyot crater.

1. Introduction

Terrestrial polygonal networks of centimetre- to decametre-scale patterned ground are common in cold-climate regions. They form by the thermal contraction of ice-cemented soils, in the case of fracture patterns, and/or the freezing and thawing of ground ice, in the case of patterned ground (e.g. Lachenbruch, 1962; Kessler and Werner, 2003). Patterned ground includes sorted patterned ground – frequently observed in periglacial environments, and thought to form through a combination of processes including frost heave and the upfreezing of clasts (Washburn, 1956; Feuillet et al., 2012) – and thermal contraction crack polygons, including various subtypes such as 'ice-wedge', 'sand-wedge', 'composite-wedge' and 'sublimation' (Marchant et al., 2002). Polygonal features have also been observed to form through the dehydration of volatile-rich material generally in arid conditions – termed desiccation polygons or desiccation cracks (Neal et al., 1968) – and through the polygonal weathering of exposed surfaces of boulders and rock outcrops (Williams and Robinson, 1989). Due to the large range of potential formation mechanisms it is important to pinpoint characteristics

* Corresponding author.
E-mail address: laura.brooker@open.ac.uk (L.M. Brooker).

https://doi.org/10.1016/j.icarus.2017.11.022

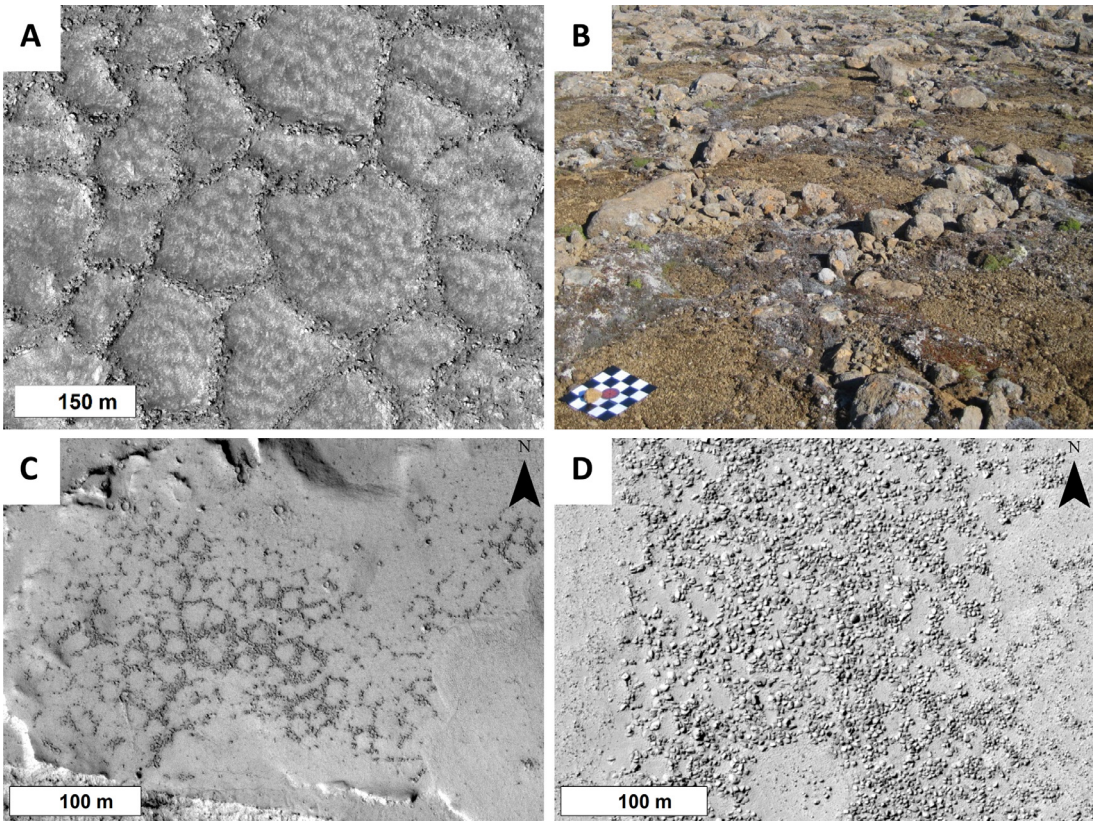

Fig. 1. A) HiRISE (ESP_016985_2315) image of part of a clastic polygonal network observed to the north-east of Lyot crater within the outer ejecta blanket. Image credit: NASA/JPL/University of Arizona. **B)** An example of morphologically similar terrestrial polygonal features found on Tindastóll Plateau, Northern Iceland. The scale is a 25 cm square with 5 cm markers. Image credit: Alex Barrett. **C)** HiRISE (PSP_004072_1845) image of possible sorted patterned ground located in the Elysium Planitia region of Mars (Balme et al., 2009). Image credit: NASA/JPL/University of Arizona. **D)** HiRISE (PSP_005597_1250) image of possible sorted patterned ground in the Argyre region of Mars (Soare et al., 2016). Image credit: NASA/JPL/University of Arizona.

unique to each polygon type to aid with identification, this is particularly key for their use as morphological (or perhaps process) analogues for features observed on Mars.

On Mars, polygonal surface features have been observed that range in diameter from metres to tens of kilometres (e.g. Pechmann, 1980; Seibert and Kargel, 2001; Mangold, 2005; Morgenstern et al., 2007; Soare et al., 2008; Lefort et al., 2009; Levy et al., 2011). Systematic study of these landforms and comparison with terrestrial analogues can help gain information into the mechanism by which they formed, and so gain insight into past and present environmental conditions. We have identified polygonal clast-bounded networks around Lyot crater, Mars. These polygons are enigmatic in that the clasts that demarcate the polygon sides are up to 15 metres across, with an average polygon diameter of 130 metres. This is significantly larger than morphologically similar polygons observed on Earth or on Mars (e.g., Fig. 1) which are found with maximum diameters of tens of metres (Washburn, 1956; Balme et al., 2009; Treml et al., 2010; Feuillet et al., 2012; Soare et al., 2016). Additionally, clastic polygons of this morphology and scale are – to our knowledge – unique to the ejecta blanket located around Lyot and so are of particular interest. Their distinctive morphology and location implies that there is a unique material and/or process leading to their formation. Thus, a better understanding of these features could provide useful information about the environment around Lyot, as well as the material that they are composed of.

The primary aim of this paper is to present the first in-depth study of these clastic polygonal features using both qualitative observations and quantitative morphometric measurements derived from high-resolution remote sensing data. Secondly, these data will be compared to both terrestrial and Martian polygon datasets collected from other studies in order to assess possible formation mechanisms and, finally, to infer a working hypothesis for their origin.

1.1. Lyot study area

Lyot crater (50°N, 30°E) is a ~215 km diameter, late-Hesperian-aged impact crater located north of Deuteronilus Mensae and immediately to the north of the dichotomy boundary. Lyot crater exhibits the lowest points of elevation in the northern hemisphere with a maximum depth of ~3 km in the crater interior (~7 km below datum). It has a central peak within an inner peak ring, and an extensive ejecta blanket composed of hummocky outer ejecta extending to ~2.5 crater radii from the crater rim, and smoother, more continuous inner ejecta with a marginal scarp which extends to ~1 crater radius from the crater rim (Fig. 2). The ejecta blanket is not well-preserved in the south and southwest due to superposition by deposits of the Deuteronilus Mensae region.

The impact event which formed Lyot crater is estimated to be late-Hesperian to early-Amazonian in age (~1.6 – 3.4 Ga; Greeley and Guest, 1987; Werner, 2008; Dickson et al., 2009). Large braided channels, extending > 300 km beyond the ejecta margins to the north, west and east of Lyot, are suggested to be the result of groundwater release during the impact event (Harrison et al., 2010). There are also numerous small channels present within the crater interior and inner ejecta blanket that are attributed to more recent fluvial activity, possibly associated with obliquity-driven climate cycles (Dickson et al., 2009; Fassett et al., 2010; Hobley et al., 2014).

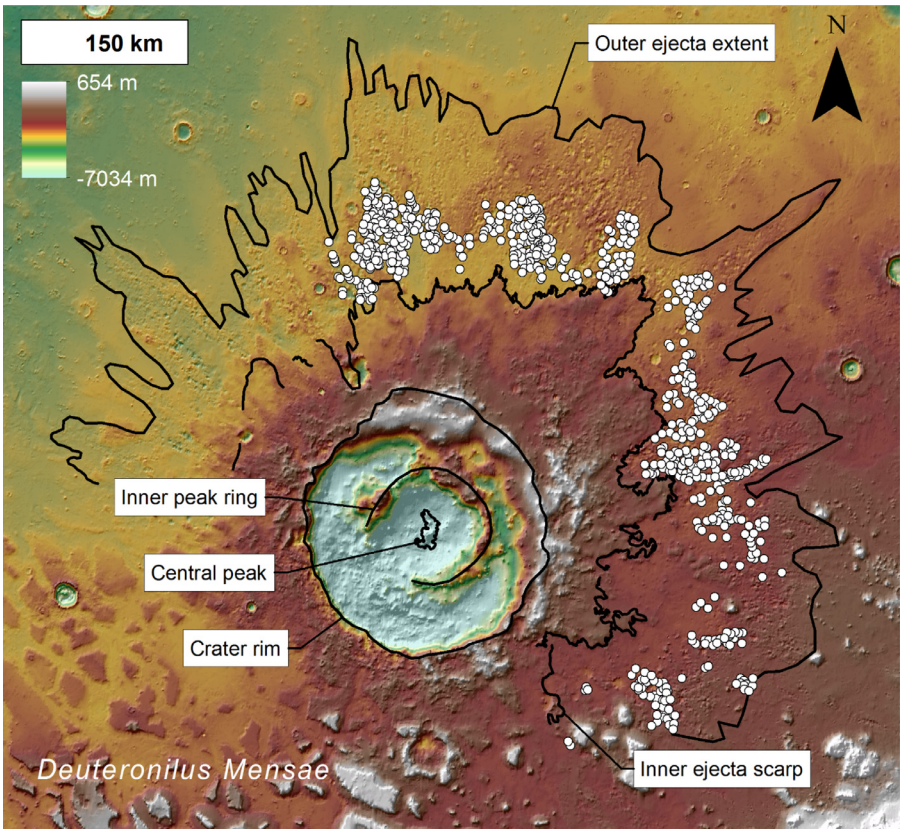

Fig. 2. Lyot crater study area displayed using colourised Mars Orbiter Laser Altimeter (MOLA; Zuber et al., 1992) topographic data overlain on a MOLA hillshade. The crater peak, inner peak ring, crater rim, inner ejecta scarp and outer ejecta extent are indicated by black lines. Regions of clastic polygonal features are marked as white circles. Image credit: MOLA Science Team.

Landforms and landscapes morphologically similar to those formed by glacial and/or periglacial processes have also been located in and around Lyot crater. These include Viscous Flow Features (VFFs) thought to be analogous to glacial landforms on Earth (Dickson et al., 2009; Balme et al., 2013; Hobley et al., 2014), mantling deposits thought to be formed by a dusty, ice-rich material (Hobley et al., 2014), and polygonal networks, as described above. Thus, it appears that the surface in and around Lyot crater has experienced the action of both ancient water sourced from underground, and recent water, probably sourced from the atmosphere (Dickson et al., 2009; Harrison et al., 2010; Hobley et al., 2014).

The clastic polygonal landforms (Figs. 1 and 2) are located only in the outer ejecta within a band ranging from the north to southeast. The polygons are of particular interest as they are much larger than most terrestrial clastic polygons and those heretofore reported on Mars (e.g. Balme et al., 2009; Gallagher et al., 2011; Soare et al., 2016), and are located in a very specific area: this pattern could indicate a genetic link between their formation and the Lyot-forming impact event.

2. Terrestrial polygon types

There is a large variety of processes that result in the production of polygonal features on Earth at a range of scales. The most widespread decametre-scale types include sorted patterned ground, thermal contraction cracks and desiccation polygons. These polygonal landforms generally do not exceed polygon diameters of ~300 metres (Neal et al., 1968). In this section, we detail the morphological characteristics and possible formation mechanisms associated with each polygon type.

2.1. Sorted patterned ground

Sorted patterned ground (e.g., Figs. 3 and 4) is composed of material sorted into coarse and fine domains which form distinctive geometric shapes including circles, polygons and stripes (e.g., Washburn, 1956; Kessler and Werner, 2003; Treml et al., 2010; Feuillet et al., 2012). Patterned ground is most commonly found in cold-climate conditions where repeated freezing and thawing cycles occur, but the exact formation mechanism is still not well understood (Washburn, 1956; Treml et al., 2010; Feuillet et al., 2012).

Frost heave, a process by which clasts may be moved to the surface, is thought to be important in the development of sorted patterned ground. There are two proposed mechanisms by which heaving occurs (Washburn, 1956; MacKay, 1984; French, 2007). The first mechanism, termed “frost-pull”, involves the growth of ice lenses by downward freezing. This ‘grips’ the clast and the overall heave of the ground leads to it being moved upwards (MacKay, 1984; French, 2007). The second mechanism, termed “frost-push”, leads to the clast being forced upwards by the forming of ice beneath it due to the greater thermal conductivity of the clast compared to surrounding material (MacKay, 1984; French, 2007). Frost heave also leads to the expansion of soil perpendicular to the freezing front causing surface clasts to migrate to clastic borders (Kessler and Werner, 2003). Over time and repeated freeze-thaw cycles, this leads to the separation of fine material from coarse material leading to raised and potentially imbricated borders (Dahl, 1966; Kessler and Werner, 2003; Soare et al., 2016). Another recognisable feature of this process is the tilting of stones due to differential heave at the top and bottom of the clast (French, 2007).

The transition between different geometric sorted forms is the result of a variety of factors including slope gradient and

Fig. 3. A) Sorted stone circles from Brøgger Peninsular on the west coast of Spitsbergen, Svalbard, Norway. The pole is approximately 1.25 metres tall. Image credit: Matt Balme. **B)** Sorted stone polygons from the western side of Hafnarfjalt, W. Iceland. Image credit: Susan Conway.

Fig. 4. Sorted stripes from the western side of Hafnarfjalt, W. Iceland. Image credit: Susan Conway.

lateral frost heave (Kessler and Werner, 2003; French, 2007; Feuillet et al., 2012). Of particular interest is the transition from circles and polygons to stripes. Stripes (Fig. 4) are composed of parallel lines of alternating coarse and fine domains oriented down slope (Washburn, 1956). Sorted polygons merge into stripes through a transition gradient of 3° to 7° (Washburn, 1956). According to Goldthwait (1976), polygons and nets form on slopes of 2° to 4°, ellipses form on 3° to 6° slopes and stripes occur on slopes of 4° to 11°

Sorted polygons generally range in diameter from 1 to 3 metres, with maximum diameters of 10 metres (Washburn, 1956; Treml, 2010; Feuillet et al., 2012). It has been suggested that the larger polygonal structures (> 3 metres in diameter) have a polygenetic origin in which pre-existing desiccation or thermal contraction cracks are exploited (French, 2007; Treml et al., 2010). Due to the presence of clasts at the polygon boundaries, polygons of this type are generally denoted as "low-centred", meaning that the polygon edges are topographically higher than the polygon centre. Another indicator of this polygon type is that the size of the clasts within the polygon borders increases with the size of the polygon, as has been observed on Earth (Washburn, 1956; Goldthwait, 1976; Bertran et al., 2010). Goldthwait (1976), for example, suggests a ratio between the polygon diameter and mean clast size of between 1:5 and 1:10.

2.2. Thermal contraction crack polygons

Thermal contraction cracks (Fig. 5) are the most widespread polygonal feature found in permafrost regions (Black, 1976; French, 2007). They can be separated broadly into the subtypes ice-wedge, sand-wedge, composite-wedge and sublimation polygons.

Thermal contraction of ground materials occurs as a result of low (below-zero) temperatures and rapid cooling, resulting in the contraction and expansion of the ground (Lachenbruch, 1962; French, 2007). Cracks form when the tensile stress due to contraction on cooling exceeds the tensile strength of the material (Lachenbruch, 1962; Haltigin et al., 2012). This is particularly prevalent in ice-cemented material as the expansion coefficient of ice is far higher than that of most silicates (Greene, 1963) and the tensile strength relatively low compared to rocks. Therefore, ice-cemented material is more likely to result in significant thermal contraction cracking where cold sub-zero air temperatures are present and where temperature losses are rapid (Lachenbruch, 1962; French, 2007).

Thermal contraction cracks form polygonal networks with average diameters in unconsolidated sediments of 10′s of metres; in consolidated bedrock, they form smaller polygons of maximum size of 5 to 15 metres (French, 2007). Theoretically, the intersection of a crack with another pre-existing crack should tend towards orthogonal angles of intersection (Lachenbruch, 1962; Plug and Werner, 2001). This implies that for angular intersections of 120° to occur, cracks must develop at a series of points almost simultaneously (French, 2007). It has also been observed in the Dry Valleys of Antarctica that young polygons have a range of sizes and tend to be relatively large with orthogonal intersections. More mature networks, however, tend towards intersections of 120° with smaller, more regularly sized polygons (Sletten et al., 2003). This indicates that the maturity of a polygonal network may be indicated by the angle of intersection and the regularity of polygon size. The various thermal contraction polygon subtypes result from different subsurface properties and environmental conditions leading to an alternate evolution of the original fracture (Black, 1976; Levy et al., 2008a).

Ice-wedges form as a result of the refreezing of water derived from melting snow, and/or the build-up of hoar frost within the fractures (Leffingwell, 1915; Black, 1976; French, 2007). This fills the fracture and prevents re-closing, and also forms a zone of weakness that reopens yearly, building up a wedge of ice over a period of tens to thousands of years (Leffingwell, 1915; Lachenbruch, 1962; Plug and Werner, 2001). The formation of the ice wedge can cause deformation of the surrounding material, resulting in raised rims on either side of the fracture

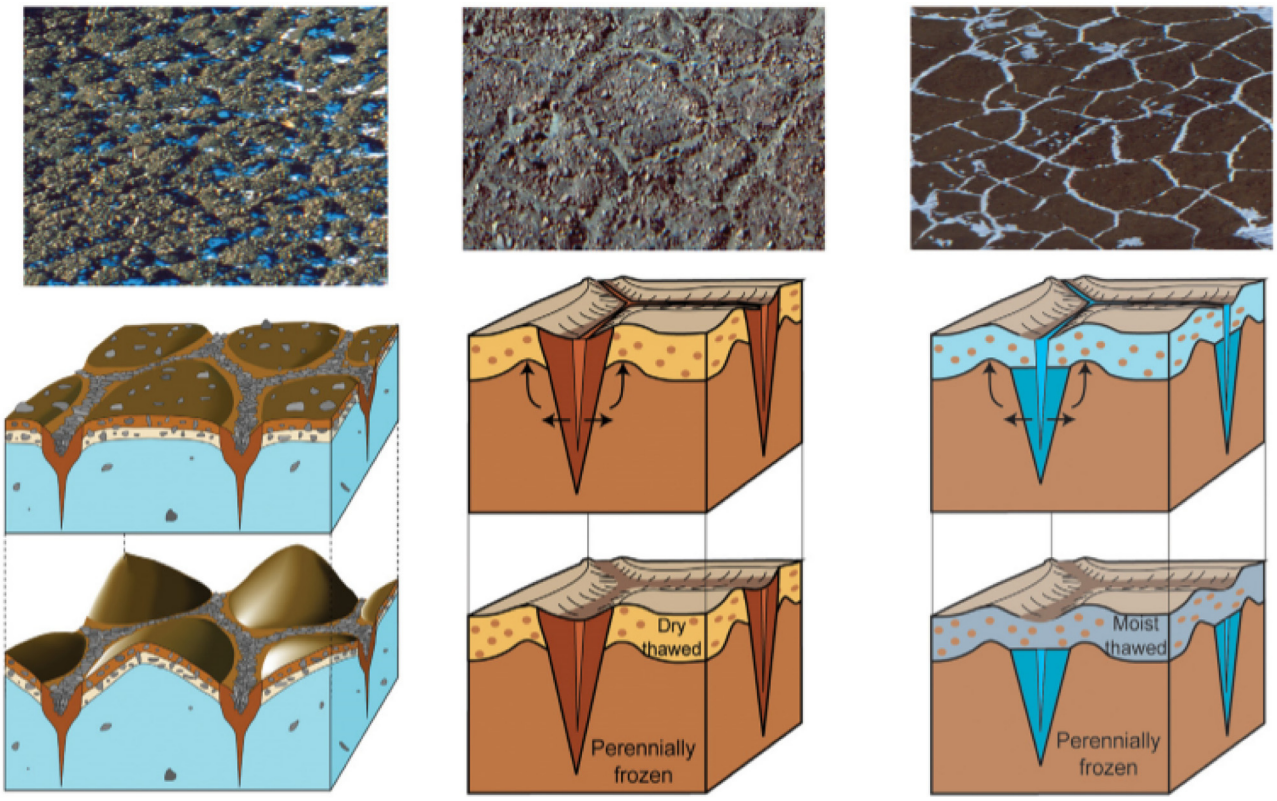

Fig. 5. Figure adapted from Fig. 6, Marchant and Head (2007). **A)** (Top to bottom) shows a photograph of sublimation polygons from the Antarctic Dry Valleys (FOV ~50 m) and a block diagram indicating how they might develop. **B)** (Top to bottom) shows a photograph of sand-wedge polygons from the Antarctic Dry Valleys (FOV ~100 m) and a block diagram indicating how they might develop. **C)** (Top to bottom) shows a photograph of ice-wedge polygons from the Antarctic Dry Valleys (FOV ~50 m) and a block diagram indicating how they might develop.

(Lachenbruch, 1962; Plug and Werner, 2001; French, 2007; Haltigin et al., 2012). French (2007) also suggests that deformation could be the result of material being pushed laterally away from the polygon centre and piling up at the margins. Ice-wedge polygons (Fig. 5C) require moisture to form and so are less likely to occur in very arid environments (Black, 1976; French, 2007).

Sand-wedge polygons (Fig. 5B) occur in cold, arid conditions (Black, 1976; Sletten et al., 2003; French, 2007). Ice is found as pore ice within the sediment at a value of less than 30% by volume (Marchant and Head, 2007). They form when wind-blown sediment infills the fracture, preventing full closure (Sletten et al., 2003; French, 2007). Like the ice-wedge case, sand-wedges cause a build-up of stresses resulting in deformation of the ground on either side of the fracture, thus forming ridges (Sletten et al., 2003). As in the case of ice-wedge polygons, sand-wedge polygons will reopen in cold conditions, and further infill of surface wind-blown material leads to the growth of the wedge, causing more defined rims to form (Sletten et al., 2003). In some cases, layers of both sand and ice will be added to the wedge due to variations in humidity, leading to the formation of composite-wedge polygons (Black, 1976; Levy et al., 2008b).

It is difficult to differentiate between ice-wedge, sand-wedge and composite-wedge polygons from surface morphology alone, as the surface expression could be similar in each case (Black, 1976; Sletten et al., 2003). All of these polygon types express an initially "high-centred" appearance, meaning that the polygon borders are demarcated by troughs surrounding the polygon centres. Over time, as the surface material is forced upwards on either side of the fractures, the polygons take on a low-centred appearance and in some cases gain 'double-rim' margins (Black, 1976; French, 2007). An additional effect of these processes is the realigning of clasts adjacent to the fracture (Black, 1976). Clastic material near to the fracture may slump into the depression (Levy et al., 2010), which could lead to a clastic border. It is worth noting that if the wedge is composed of ice, removal of this ice (i.e. through thaw or sublimation) results in the slumping of surface material into the fracture, leading to collapse structures and resulting in a high-centred appearance (Washburn, 1956; Black, 1976; Sletten et al., 2003; Levy et al., 2010; Ulrich et al., 2011). Ice-wedge polygons have a typical diameter range of 10 to 40 metres with maximum diameters of over 100 metres occasionally seen (Washburn, 1956; Black, 1976; Washburn, 1980). The diameters of sand-wedge and composite-wedge polygons are similar, due to similar formation mechanisms.

Sublimation polygons (Fig. 5A) occur in locations where there is excess ice in the shallow subsurface in an environment with no wet active layer (Marchant and Head, 2007). On Earth, sublimation polygons are uncommon and occur in the Dry Valleys, Antarctica, where they are underlain by massive ice (Marchant and Head, 2007). As cracks form in the underlying ice, debris overlying the fracture can collapse into the depression, resulting in coarse-grained debris at polygon borders (Marchant et al., 2002; Marchant and Head, 2007; Levy et al., 2010; Haltigin et al., 2012). This in turn increases the rate of sublimation beneath, leading to the development of deep troughs and the typically high-centred appearance of this polygon subtype (Marchant et al., 2002; Sletten et al., 2003; Levy et al., 2006; Marchant and Head, 2007; Levy et al., 2010). The location of ice in the subsurface significantly impacts polygon morphology, as does the aspect of the slope that they are forming on (Marchant et al., 2002; Levy et al., 2008a). Sublimation polygons in Beacon Valley, Antarctica, have diameters ranging from 6 to 35 metres (Marchant et al., 2002; Levy et al., 2008a). Subli-

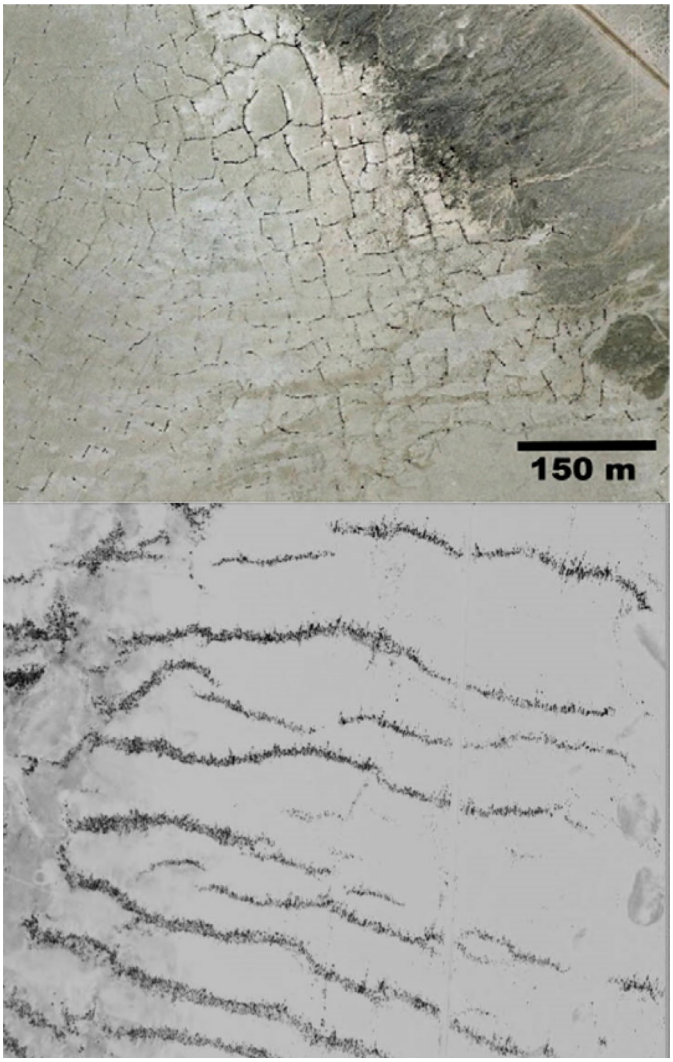

Fig. 6. A) Image showing large desiccation cracks from Coyote Lake, California. After Fig. 1A, El Maarry et al. (2012). **B)** Image showing desiccation stripes, ~ 400 metres in length, from the Indian Springs Playa, Nevada. After Fig. 8, El Maarry et al. (2010).

mation polygons tend to be smaller in diameter than sand-wedge polygons where the two occur in similar environmental conditions (Levy et al., 2006; Levy et al., 2010).

2.3. Desiccation polygons

Desiccation polygons (Fig. 6) are commonly found in arid playa environments where the ground is extremely hard and flat (Neal et al., 1968; Loope and Haverland, 1988). They generally form in lacustrine deposits composed of fine grained aeolian material, which are able to accommodate a significant amount of volatile material (Neal et al., 1968; Loope and Haverland, 1988; El Maarry et al., 2010; El Maarry et al., 2012; El Maarry et al., 2014).

Desiccation cracks form as a result of volume loss due to the evaporation or diffusion of volatiles such as ice or water as summarised by El Maarry et al. (2012) and El Maarry et al. (2014). This volume loss causes a change in surface tension between grains, resulting in a build-up of stress (El Maarry et al., 2010; El Maarry et al., 2012). Once this stress exceeds the strength of the ground material, a fracture can form (Neal et al., 1968; Weinberger, 2001; El Maarry et al., 2010). Fractures take months to years to develop as seasonal flooding only permeates shallowly into hard playa material (Neal et al., 1968). Once they form, desiccation fractures are generally irregular, jagged and less than 30 cm wide (Neal et al., 1968). Young fractures are discontinuous and material may slump into them (Neal et al., 1968). Secondary fractures develop at right angles to the initial fracture, leading to polygonal patterns with orthogonal intersections in plan-view (Neal et al., 1968; Loope and Haverland, 1988; Weinberger, 2001). Non-orthogonal intersections can occur either as a result of the development of a series of fractures simultaneously in a homogenous material (El Maarry et al., 2014), or the maturation of a network from the repeated opening and closing of fractures due to recurrent wetting and drying (Neal et al., 1968; Loope and Haverland, 1988). Further contraction fracturing often subdivides large polygons into regular, smaller polygons giving a nested appearance (El Maarry et al., 2014).

Desiccation polygons occur across a range of scales. Primary desiccation fracture polygons rarely exceed diameters of 1 metre (Lachenbruch, 1962; Loope and Haverland, 1988; El Maarry et al., 2014), although much larger polygons have been observed in some playa basins (e.g. Fig. 6A). These polygons can have diameters of between 15 to 100 metres, or even up to 300 metres (Neal et al., 1968). As polygon diameter is related to the thickness of the layer subject to fracturing, the stressed region needs to be thick to produce larger polygons (Neal et al., 1968; Groisman and Kaplan, 1994; El Maarry et al., 2014). It is thought that large desiccation polygons occur as a result of intense evaporation due to a period of increased aridity, combined with lowering of the ground-water level as a result of geological and/or human activity (Neal et al., 1968; El Maarry et al., 2012). The fissuring process might be aided by gradual subsidence or sudden earthquakes (Neal et al., 1968).

Desiccation polygons typically exhibit a pentagonal to hexagonal appearance (Neal et al., 1968; Weinberger, 2001; El Maarry et al., 2014). They can grade into stripes or parallel fractures as a result of constriction in narrow zones (Fig. 6B; Neal et al., 1968). Desiccation polygon centres are often depressed relative to the polygon lip, and at intersections a collapse hole is often visible (Neal et al., 1968). Over time, wind-blown material will fill these fractures leading to a surface “stain” even when the topographic signature of the fracture is not visible (Neal et al., 1968).

3. Data and methods

3.1. Data

Observations of landforms and landscapes in and around Lyot crater, indicate that clastic polygons are recognisable as organised, rough-textured features with clasts demarcated by dark shadows in 6 m/pixel context camera (CTX) images (Fig. 7; Malin et al., 2007). Although CTX data is suitable for the mapping of clastic polygonal networks, it is not suitable for an in-depth study of these polygons, since the clasts which demarcate polygon edges are generally beneath the resolution of the data. Due to this, higher resolution images from the High Resolution Imaging Science Experiment (HiRISE) have been chosen for use in this study.

HiRISE data has a ground pixel size of 0.25 to 1.3 m/pixel allowing metre-scale objects to be resolved (McEwen et al., 2007), although the spatial coverage for this dataset is low on the global scale. In addition, where HiRISE stereopairs are available, digital elevation models (DEMs) and orthoimages can be produced (Kirk et al., 2008). This allows information such as slope and aspect to be extracted from the data.

Six areas or ‘strips’ were identified as having HiRISE image coverage suitable for use in this study (Fig. 8). These images cover clastic polygonal networks to the north and northeast of Lyot crater, with five strips clustered in a similar location. One of the strips has a HiRISE stereopair available (ESP_03,3059_2345 and ESP_03,2980_2345); where other images are absent of repeated stereo cover, CTX stereopairs

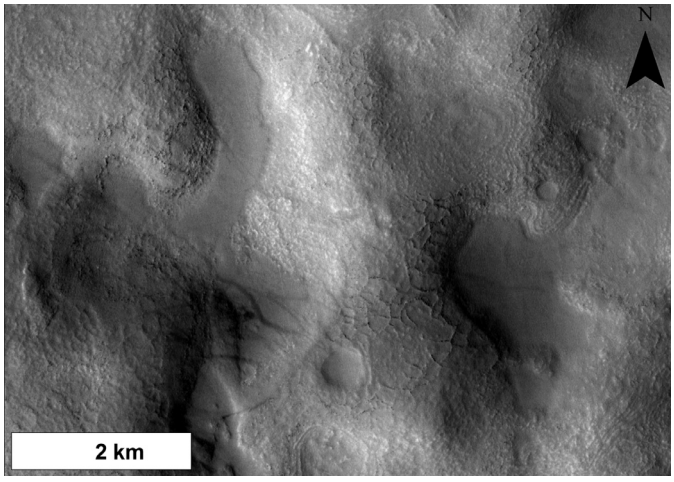

Fig. 7. CTX image (B17_016484_2346) showing a section of a clastic polygonal network visible as organised, rough textured, polygonal features. The presence of clasts is inferred both by comparison of similar features in HiRISE images and from the dark shadows that are cast by the polygon margins. Image credit: NASA/JPL-Caltech/MSSS.

(B19_01,6985_2338 and B21_01,7697_2303, B19_01,6906_2346 and D15_03,3059_2344) have been used instead (Fig. 8). The method of producing DEMs from stereopairs is described by Kirk et al. (2008), and we have followed that approach here. DEMs used within this study were generated using SOCETSET software. The HiRISE DEM so produced has a grid spacing of 1 metre, whereas the CTX DEMs have grid spacings of 18 metres. For analysis of aspect and slope, the DEMs were smoothed using a moving-window running mean to remove the effects of small topographic features, with a window size of 100 metres for the HiRISE DEM and 400 metres for the CTX DEMs. Slope and aspect maps were derived from the smoothed HiRISE and CTX DEMs. All morphometric measurements and post-DEM processing was performed using ArcGIS 10.1 software.

3.2. Morphometric analyses

To collect morphometric data, the observed polygons must be digitised and analysed. Our method of analysis is based upon that of Ulrich et al. (2011), who used a similar technique to digitise thermal contraction fracture networks. Clastic polygonal networks were manually digitised onto HiRISE data using ArcMap 10.1 software using a Cassini projection centred on the 30° east meridian. Only polygonal networks in which the polygons could be reliably interpreted as clastic were mapped. This was done by digitising polygon margins down their centre-lines with the start and end points corresponding to the intersection of other polygon edges or a lack of further clasts. If all of the lines formed a continuous, closed feature then this was considered to be a clastic polygon. All the candidate clastic polygons visible in each strip were examined and digitised.

The overlaying of mantling deposits on the polygons can make it challenging to identify whether clasts are present, as well as obscuring the polygon geometry. If there was a high level of uncertainty surrounding the identification of a clastic polygon edge it was left unmarked.

Once each strip was completely digitised, morphometric parameters were calculated and extracted using a tool written in the Python scripting language for use with ArcMap. The key parameters extracted are listed in Table 1. Fig. 9 illustrates how the values are extracted for a typical clastic polygon. In addition, the length and width of the five largest clasts in a polygon were measured for fifteen randomly selected polygons from each strip. These measurements were made manually within ArcMap, with the clasts se-

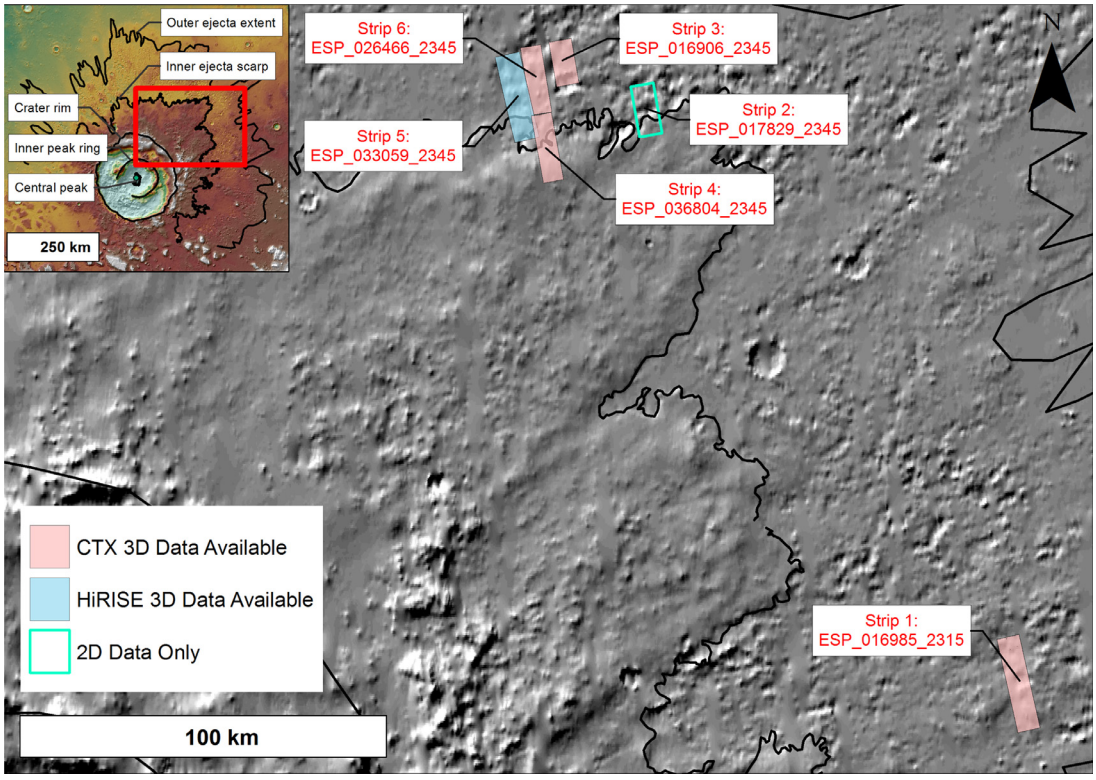

Fig. 8. The red box within the inset map indicates the extent of the main image. The background is a MOLA hillshade. The strips are labelled according to the naming convention used in this study. Black lines indicate the crater rim, inner ejecta scarp and outer ejecta extent. Image credit: MOLA Science Team.

Table 1
Morphometric parameters and topographic properties extracted and calculated for each polygon network digitised. The parameters selected are based upon those used by Ulrich et al. (2011).

Parameter	Data Source	Description
Number of sides	HiRISE	The number of sides is extracted from simplified polygons.
Length (m)	HiRISE	The length of the longest axis of the simplified polygon.
Width (m)	HiRISE	The length of the minor axis of the simplified polygon.
Perimeter (m)	HiRISE	The length of all of the polygon sides added together.
Area (m^2)	HiRISE	The area enclosed within the polygon.
Orientation (°)	HiRISE	The orientation of the longest polygon axis with values of between 0 and 180° measured from true north.
Size (m)	HiRISE	$= \sqrt{\frac{4A}{\pi}}$ where A is the polygon area.
Circularity	HiRISE	$= \frac{4\pi A}{P2}$ where A is the polygon area and P is the polygon perimeter. 0 indicates an elongate ellipse and 1 indicates a circle.
Distance from crater centre (km)	HiRISE	The distance measured from Lyot crater centre to the centre of the polygon.
Intersection Type	HiRISE	A count of the number of sides meeting at each polygon vertex.
Intersection Angle (°)	HiRISE	The angle between the sides at an intersection.
Clast Length (m) (for 15 polygons per strip)	HiRISE	The length of the longest axis of the five largest clasts.
Clast Width (m) (for 15 polygons per strip)	HiRISE	The length of the minor axis of the five largest clasts.
Clast Size (m) (for 15 polygons per strip)	HiRISE	$= \sqrt{\frac{4A}{\pi}}$ for the five largest clasts where A is the clast area.
Mean slope (°)	Smoothed HiRISE or CTX DEM	The mean slope across the area of the polygon.
Mean aspect (°)	Smoothed HiRISE or CTX DEM	The mean aspect across the area of the polygon.

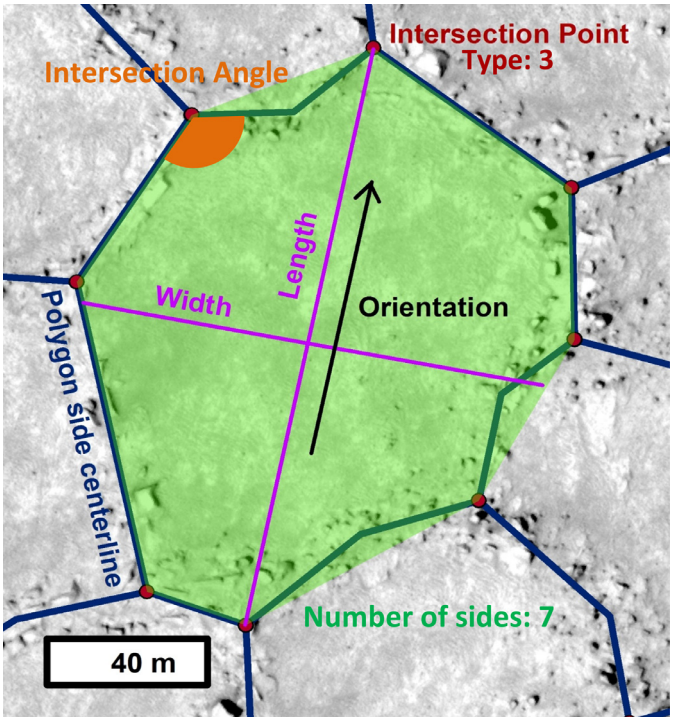

Fig. 9. HiRISE (ESP_016985_2315) image of a digitised clastic polygon from the Lyot study area with the scheme of the key extracted values displayed (listed in Table 1). The green shaded area indicates the minimum bounding area of the polygon which takes the form of a simplified polygon. This is used to extract length, width, orientation and the number of sides. The polygon area is taken as the area within the blue digitised lines, and the perimeter is taken as the lengths of each of the blue lines added together. Other values such as size and circularity are calculated from the extracted values. Image credit: NASA/JPL/University of Arizona.

lected by observing which are the largest within the polygon at a high zoom level.

The parameters chosen were based upon those selected by Ulrich et al. (2011), as well as other studies of polygonal networks (Neal et al., 1968; Yoshikawa, 2003; Burr et al., 2005; Treml et al., 2010; Barrett, 2014). The digitised parameters were automatically added as an attribute table attached to the digitised polygons and then exported so that statistical values could be calculated (e.g., mean, minimum, maximum, first quartile, median, third quartile, standard deviations and skewness values). All graphs were created using R (R Core Team, 2013) within RStudio (RStudio Team, 2015).

4. Observations and results

Six strips of HiRISE data were surveyed for clastic polygonal networks, with a total of 3588 polygons digitised, of which 3197 occur within available, high resolution topographic data (HiRISE or CTX DEMs). During the digitisation process, clastic polygonal features were also scrutinised for morphological features that might provide insight into their formation process. This section is therefore divided into qualitative observations and quantitative morphometric data.

4.1. Polygon observations

Clastic polygonal features are recognisable on both CTX and HiRISE data as comparatively rough-textured, patterned areas, surrounded by dark shadows cast by the clasts. In HiRISE images, individual clasts can be easily seen. The polygons are located within areas of terrain with kilometre scale hummocky relief. They are constrained to the higher topography at the upper parts of the hummocks; depressed areas are marked by a lack of polygonal features. However, it should be noted that many of the depressions found near to the polygonal networks contain infilling, smooth, mantling deposits, which could obscure polygonal features (Fig. 10).

The networks themselves appear to change shape in relation to differences in topography, with clastic polygons “bending” around depressions (Fig. 10A) and occasionally becoming drawn out into small boulder fields in constricted regions (Fig. 10B). Equally, clastic polygons can be seen to form oriented patterns on and around higher topography features (Fig. 10B). Towards the boundary of the network, the edges become discontinuous and isolated polygons are observed, many of which appear nearer circular in shape (Fig. 11A). In some locations, the polygonal networks do not grade into discontinuous forms, but instead become draped by mantling deposits which obscure the clasts (Fig. 11B).

In addition to the areas of clastic polygonal ground, large boulder fields occur within the outer ejecta blanket of Lyot crater, which have a similarly distinctive topographic relationship with

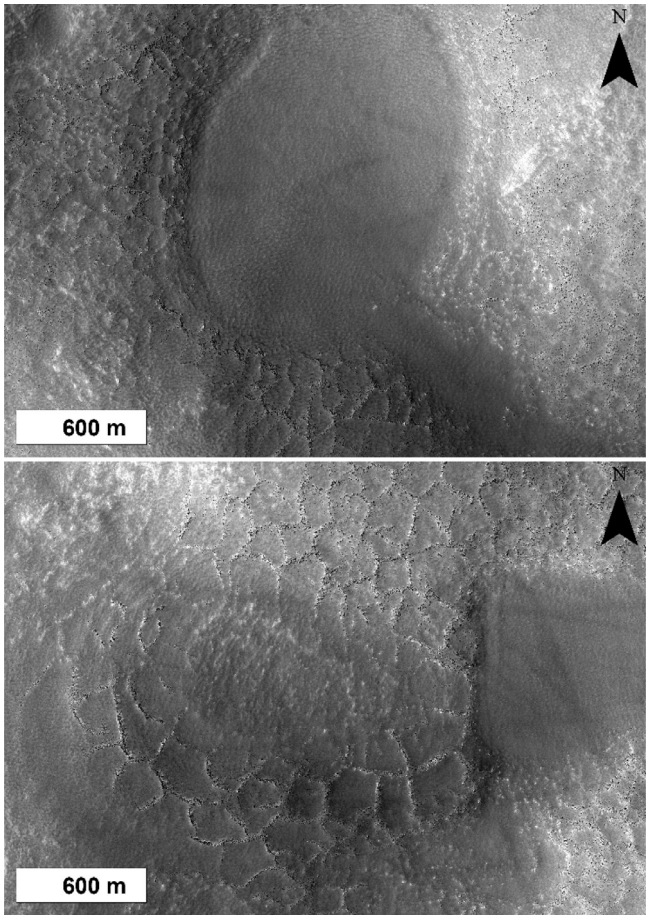

Fig. 10. A) HiRISE (ESP_026466_2345) image of clastic polygons "bending" around a large depressed region infilled with a smooth, mantling unit. **B)** HiRISE (ESP_016985_2345) image of clastic polygons oriented around a higher topographic feature. Clasts to the east of the high topographic feature have been drawn out as a result of constriction between the depressed region and the area of higher topography. Image credit: NASA/JPL/University of Arizona.

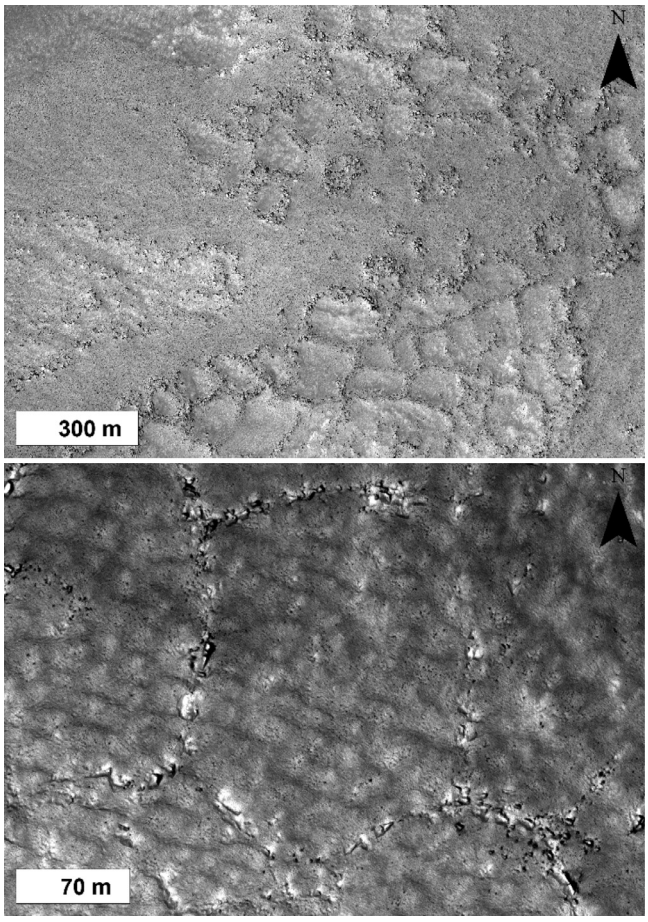

Fig. 11. A) HiRISE (ESP_019685_2315) image of the edge of a clastic polygonal network which appears to become discontinuous, with isolated, more circular, forms being present with wider clastic borders. **B)** HiRISE (ESP_017829_2345) image of clastic polygons which appear to have become draped by a mantle deposit. Image credit: NASA/JPL/University of Arizona.

interspaced mantle-filled depressions (Fig. 12). No large boulder fields have been observed near to the polygon nets studied, although the landscape related to the polygons contains a large volume of clastic material, both within the polygons, and as a light covering of small clasts throughout the region interpreted from shadows cast by material below the resolution limit. There are some small boulder fields bordering polygonal networks but there is often a cleared boundary area between the end of the polygonal network and the start of the boulder field (Fig. 13).

The clastic polygons are often irregular in size and form, although they generally approximate hexagonal and pentagonal shapes. In many large polygons, discontinuous lines of clasts partition the interior, suggesting either that the larger polygon formed from merging smaller polygons, or that an existing large polygon was partitioned into smaller areas after it formed (Fig. 14). In such examples, the clastic line is often draped with mantle material indicating that it could continue underneath the mantling deposit. Alternatively, Soare et al. (2016) suggest that sorting could become truncated early on during the process of development, leaving the landform in adolescence. The vast majority of polygons appear to emerge from superposing mantling material. This can make identification of features associated with many terrestrial polygons, such as fractures along polygon sides, difficult.

The polygon margins are composed of clasts which range in size and form from small and approximately circular boulders, just

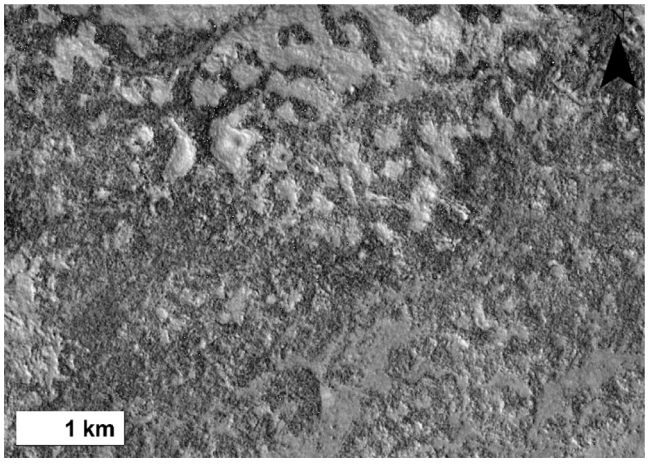

Fig. 12. CTX (B20_017552_2335) image of a large boulder field present within the outer ejecta blanket of Lyot crater. The clastic material is recognisable as a low albedo rough texture found on areas of higher topography. Clastic material bends around depressions which often contain smooth, mantle material. Image credit: NASA/JPL-Caltech/MSSS.

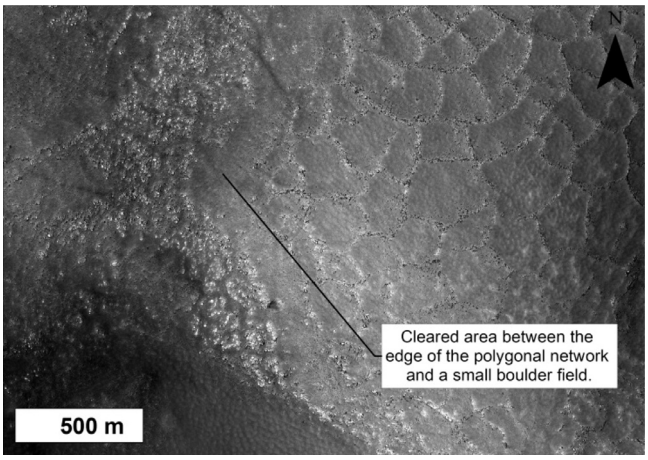

Fig. 13. HiRISE (ESP_017829_2345) image of the edge of a clastic polygonal network where a small boulder field can be observed. There is a cleared area located between the end of the polygonal network and beginning of the small boulder field. Image credit: NASA/JPL/University of Arizona.

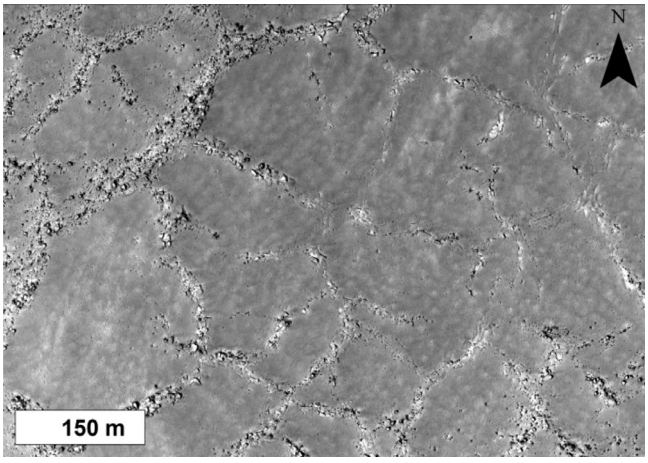

Fig. 14. HiRISE (ESP_016906_2345) image showing a large clastic polygon which contains discontinuous internal clastic lines. Due to a change in albedo of the mantle and bumps where boulders would be expected, it is indicated that smaller polygons are contained in the interior which have become overlain with mantle material. Image credit: NASA/JPL/University of Arizona.

at the image resolutions, to large and ridge-like clasts of up to 15 metres in diameter. Small boulders can also be found within some polygons (Fig. 15A). The polygon borders sometimes have a "double-rimmed" appearance, where there are two lines of clasts roughly parallel to each other, sometimes with a slight gap between them (Fig. 15B). The clasts which form the polygon edges are commonly angular with square to rectangular shapes (Fig. 15). They often line up end to end to form the polygon sides and many give the appearance that they have formed from the fracturing of larger, more elongate clasts. The topographically high clasts give the polygons a low-centred appearance (Fig. 16). No fractures or troughs have been observed to demarcate the polygon borders, although the presence of probably younger overlying mantle makes this difficult to constrain. Polygon margins are high standing and clasts do not appear to overlie or be contained within fractures of troughs (Fig. 16). Examination of many topographic-profiles (made from the best 1 m-resolution HiRISE DEM, and avoiding any possibly noisy areas) across the polygon margins show no evidence of the clasts sitting within troughs at the margins.

In summary, the clastic polygons located around Lyot crater are generally hexagonal to pentagonal in form and occur on a range of scales (see Section 3.2). They are constrained to areas of higher topography, though polygons occurring in depressed regions might be obscured by mantling units. Polygon morphology is observed to have been affected by topographic features causing them to be orientated around areas of high or low topography and become elongate in form in constricted regions. Polygon edges are commonly composed of angular clasts which can exhibit a "double-rimmed" appearance. No fractures or troughs have been observed demarcating polygon edges. Finally, we have not observed polygon networks and boulder fields being spatially adjacent within the outer ejecta blanket. This is in contrast to Earth where sorted patterned ground commonly occurs in a pre-existing clastic layer such as glacial till or blockfields (e.g. Goldthwait, 1976; Wilson and Sellier, 1995; Grab, 2002).

4.2. Morphometric data

The key morphometric data gathered from 3588 polygons are presented in Tables 2, 3 and 4. These tables provide summarised statistical values for each parameter of interest.

The clastic polygons across the six strips are relatively uniform in shape, with no statistically significant difference between the mean values recorded for the individual strips. Clastic polygons are commonly 5 to 6 sided with a mean polygon size of 130 metres. The distribution of polygon sizes in each strip is broad, indicated by the quartile ranges in Fig. 17, but as a whole the populations are fairly similar for each strip. Strips 1 and 4 appear to show a more confined normal distribution when compared to the other areas. Polygon circularity values are generally constrained to values of between 0.5 and 0.9 with a mean value of ~0.7 (Fig. 18). This indicates that polygons tend to be equidimensional rather than elongate in shape.

The polygon intersection values show a distribution centred around 120° (Fig. 19). The highest percentage of intersections (Table 3) are 3-ray (93.1%), with only 6.7% of intersections recorded as 4-ray. This indicates that the polygons tend towards equiangular nets, as opposed to orthogonal nets.

5. Analysis

5.1. Key relationship between parameters – hypothesis testing

Sorted patterned ground on Earth formed by freeze-thaw processes displays clear relationships between circularity and average slope values (Washburn, 1956; Goldthwait, 1976), aspect and polygon orientation (Washburn, 1956), and between polygon size and clast size (Washburn, 1956; Goldthwait, 1976; Bertran et al., 2010). On Earth, circularity is inversely related to underlying slope (i.e. sorted polygonal forms become elongated downslope on steeper slopes). Also, terrestrial observations indicate that larger polygons tend to have larger clast sizes in their borders (Washburn, 1956; Goldthwait, 1976; Bertran et al., 2010). We therefore investigate whether there are any relationships between polygon circularity and average slope, polygon orientation and average aspect, and polygon size and clast size, which might support a periglacial origin for the clastic polygons in Lyot.

There is no evidence for any relationship between polygon circularity and underlying slope (Fig. 20). There is also no evidence of any relationship between polygon orientation and underlying aspect, signifying that polygons are randomly oriented (Fig. 21). This indicates that the shape of polygons does not vary with slope, and therefore polygons do not appear to grade into elongate forms downslope as slope increases. This could be the result of a small amount of data available for polygons on slopes of greater than 6°; according to Goldthwait (1976), polygons and nets form on slopes of 2° to 4°, ellipses form on 3° to 6° slopes and stripes occur on

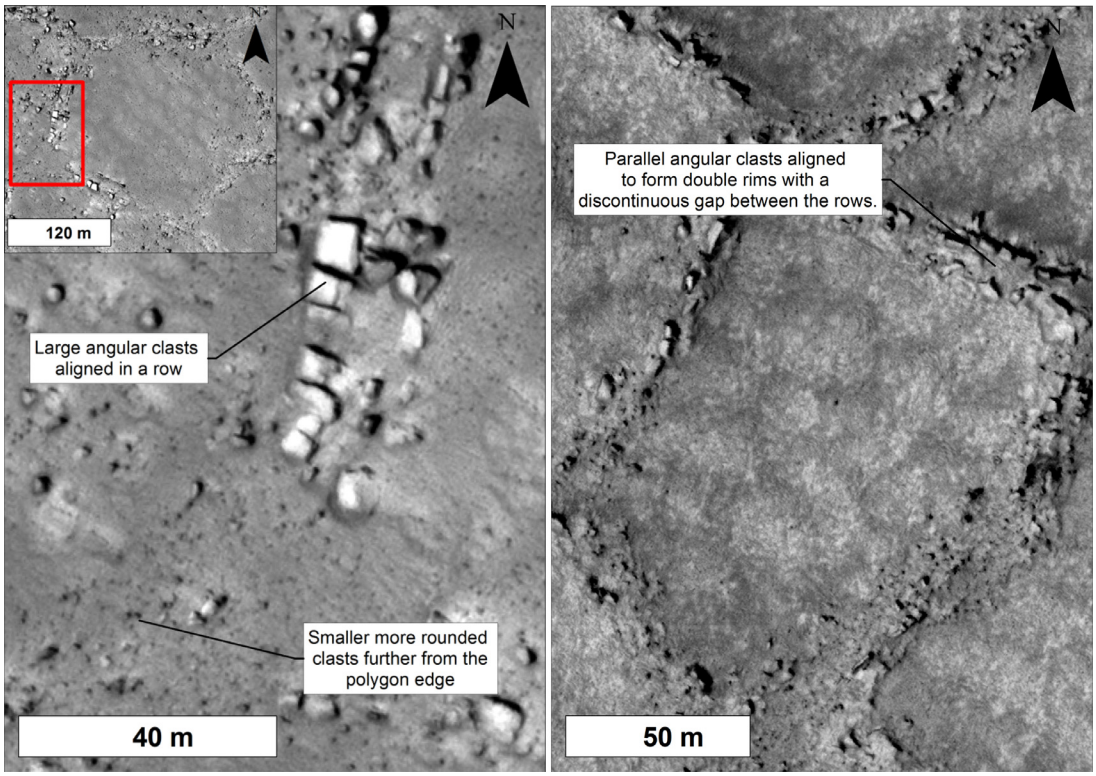

Fig. 15. A) HiRISE (ESP_017829_2345) image showing a variety of different clastic features including large angular clasts aligned in rows and smaller rounded clasts which are generally located further from polygon edges. **B)** HiRISE (ESP_016985_2315) image showing clastic polygons with double rims of parallel angular clasts, occasionally with a slight gap between them, which is characteristic of many polygon edges. Image credit: NASA/JPL/University of Arizona.

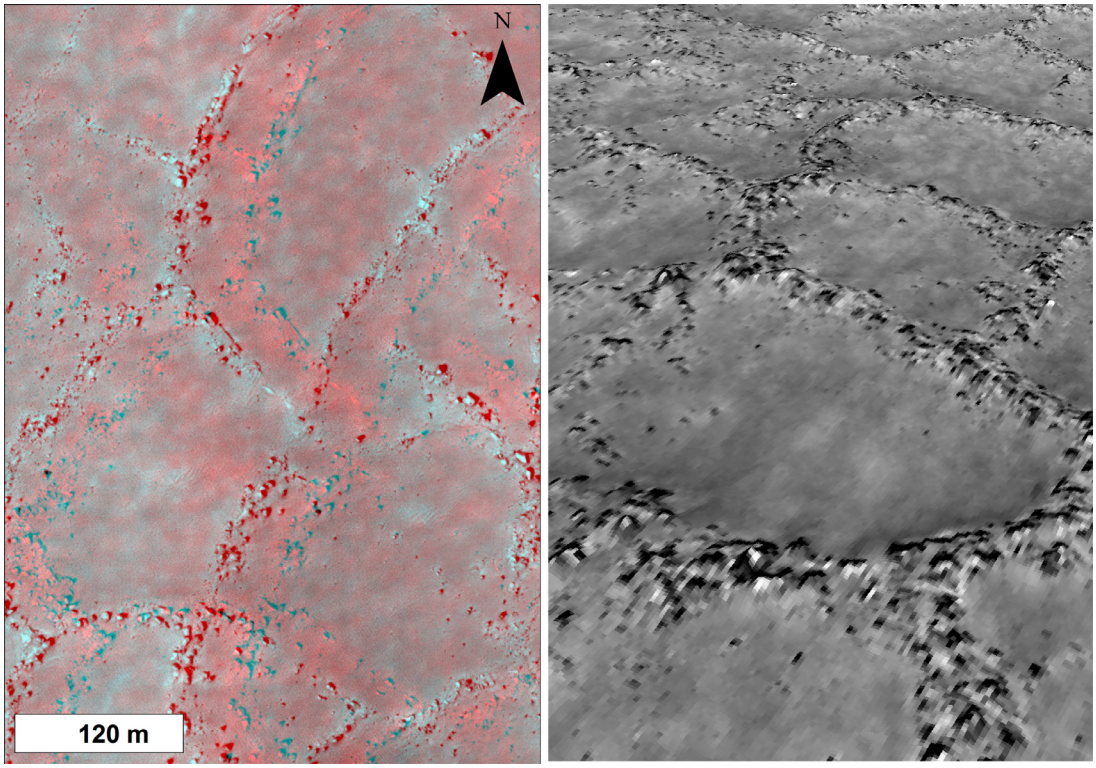

Fig. 16. A) Anaglyph (ESP_032980_2345_ESP_033059_2345) showing part of a clastic polygonal network. Scale is approximate. Image credit: NASA/JPL/University of Arizona. **B)** 3D view of part of a clastic polygonal network using an orthoimage generated from HiRISE data (ESP_032980_2345) and the corresponding 1 m/pixel DEM. There is a vertical exaggeration of 1.2. Figure created using ArcScene 10.1. Image credit: NASA/JPL/University of Arizona.

Table 2
Morphometric parameters summarised for all polygons analysed within the study.

Parameter	Length (m)	Width (m)	Size (m)	Circularity	Intersection Angle (°)	Underlying Slope (°)	Clast Length (m)	Clast Width (m)	Clast Size (m)
Mean	179	117	130	0.712	116	2	5	3	5
Maximum	676	450	435	0.966	268	12	15	10	12
Minimum	19	11	16	0.226	19	0	1	1	1
Count	3588	3588	3588	3588	21,267	3197	450	450	450
Median	172	111	126	0.727	114	2	5	3	4
1st Quartile	126	79	91	0.644	93	1	3	2	3
3rd Quartile	222	149	164	0.793	139	3	7	4	6
Standard Deviation (SD)	78.053	10.799	56.179	0.114	34.397	1.413	2.196	1.571	1.993
Skewness (SK)	1.023	0.807	0.699	−0.645	0.161	1.384	0.816	0.876	0.003

Table 3
Intersection types that occur within the polygonal networks summarised across all strips.

Intersection type	Number	Percentage
2-ray	15	0.2
3-ray	8741	93.1
4-ray	625	6.7
5-ray	8	0.1
Total	9391	100

Table 4
Number of sides per polygon.

Number of sides	Number	Percentage
3-side	236	6.8
4-side	593	17.0
5-side	912	26.1
6-side	781	22.4
7-side	503	14.4
8-side	258	7.4
9-side	144	4.1
10-side	64	1.8
Total	3491	100.00

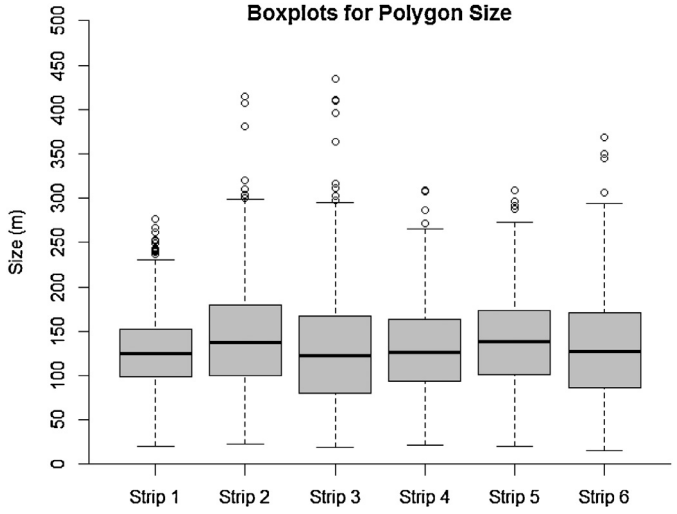

Fig. 17. Boxplots displaying polygon size values for all of the strips analysed. The boxes represent the interquartile range of each strip. The bold horizontal line is the median of each strip. The whiskers represent the upper and lower quartile. The outliers are located 1.5 times the interquartile range above the upper quartile.

slopes of 4° to 11° Finally, there is no correlation between polygon size and clast size (Fig. 22). In fact, the smallest polygons can contain the largest clasts and vice versa. These three null results, taken together, argue against the Lyot clastic forms having a periglacial, freeze-thaw origin: they do not show any of the relationship found in terrestrial freeze-thaw sorted polygons and circles.

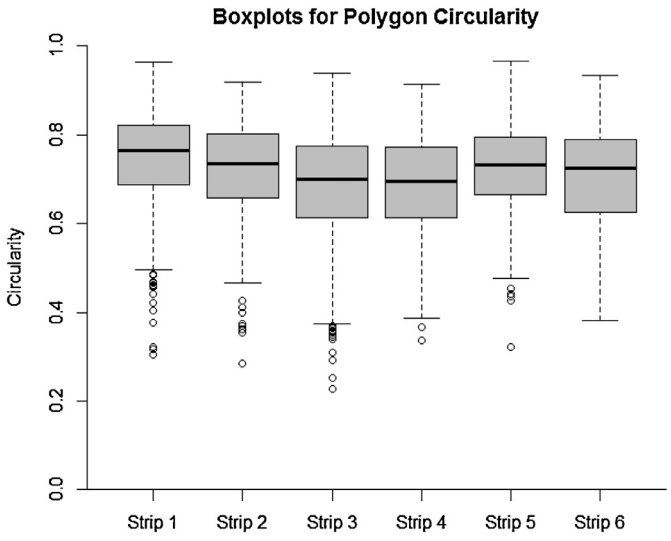

Fig. 18. Boxplots displaying polygon circularity values for all of the strips analysed. The boxes represent the interquartile range of each strip. The bold horizontal line is the median of each strip. The whiskers represent the upper and lower quartile. The outliers are located 1.5 times the interquartile range above the upper quartile.

5.2. Comparison datasets

Having obtained measurements and observations of these polygonal features, we can use these data to test hypotheses for how they formed. However, to gain additional insight into their possible formation mechanisms we also gathered comparative data for other polygonal patterned grounds, both from Earth and Mars. The various polygon datasets have been collated from the literature, and cover a variety of different polygon types including thermal contraction crack polygons, sorted patterned ground and desiccation polygons (i.e. not just positive-relief margin, clast-bounded polygons). We have done this in order to consider the widest possible suite of possible formation mechanisms. For example, it could be imagined that negative-relief margin (i.e., trough or fracture-bounded) polygons could become infilled by clasts or debris and then inverted by differential erosion to form features similar to those seen here. Hence, we need to consider many types of polygonal ground. However, it has been difficult to locate morphometric measurements of similar detail to those conducted in either this study or that of Ulrich et al. (2011). Accurate intersection angle and clast size data has been particularly challenging to locate. As a result, many parameters do not have comparison data available.

First, we consider the basic plan-view shape and size of the Lyot polygons. Fig. 23 shows mean polygon size values plotted against mean circularity for each strip. The comparison data include small thermal contraction crack polygons from Earth and Mars (Ulrich et al., 2011), and sorted patterned ground from Earth

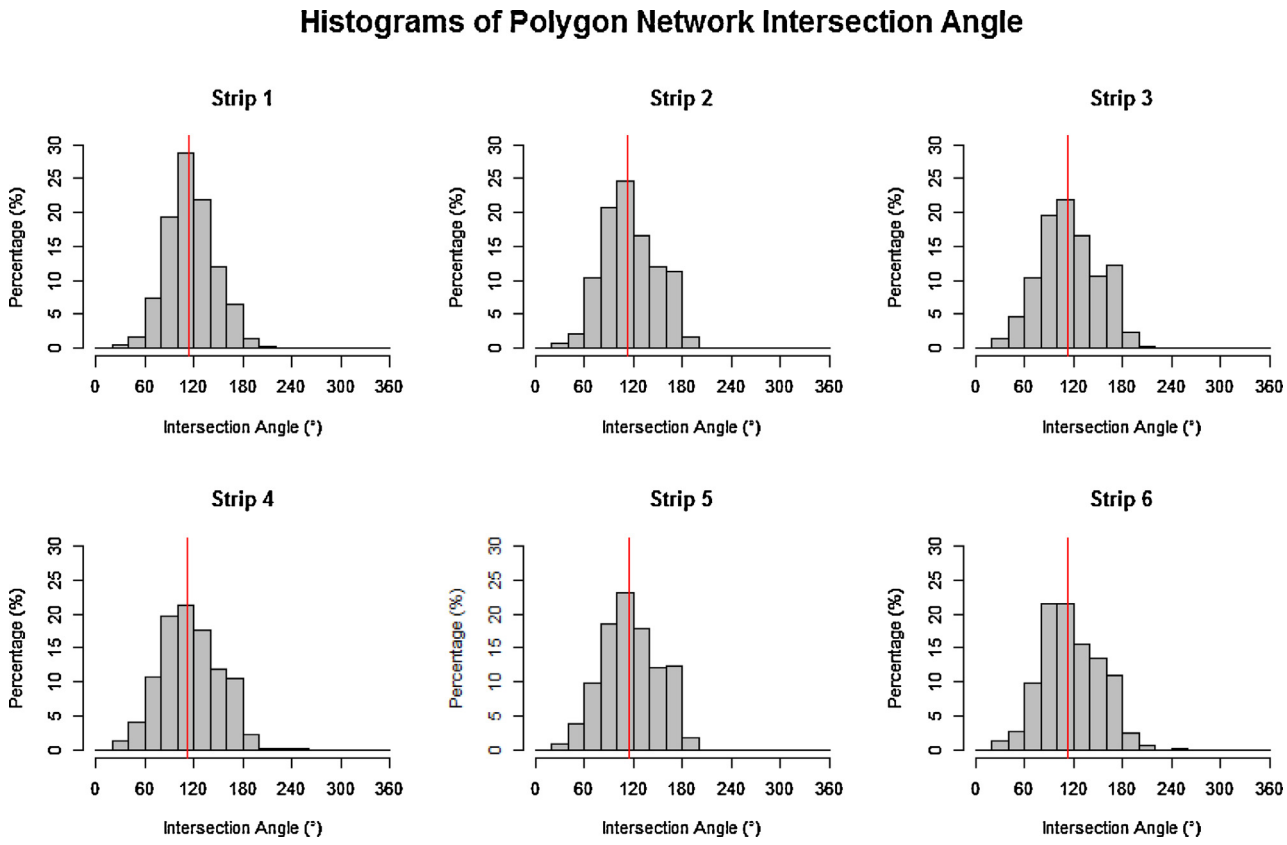

Fig. 19. Histograms displaying polygon intersection angle values for each of the strips analysed. The median for each strip is marked as a red line.

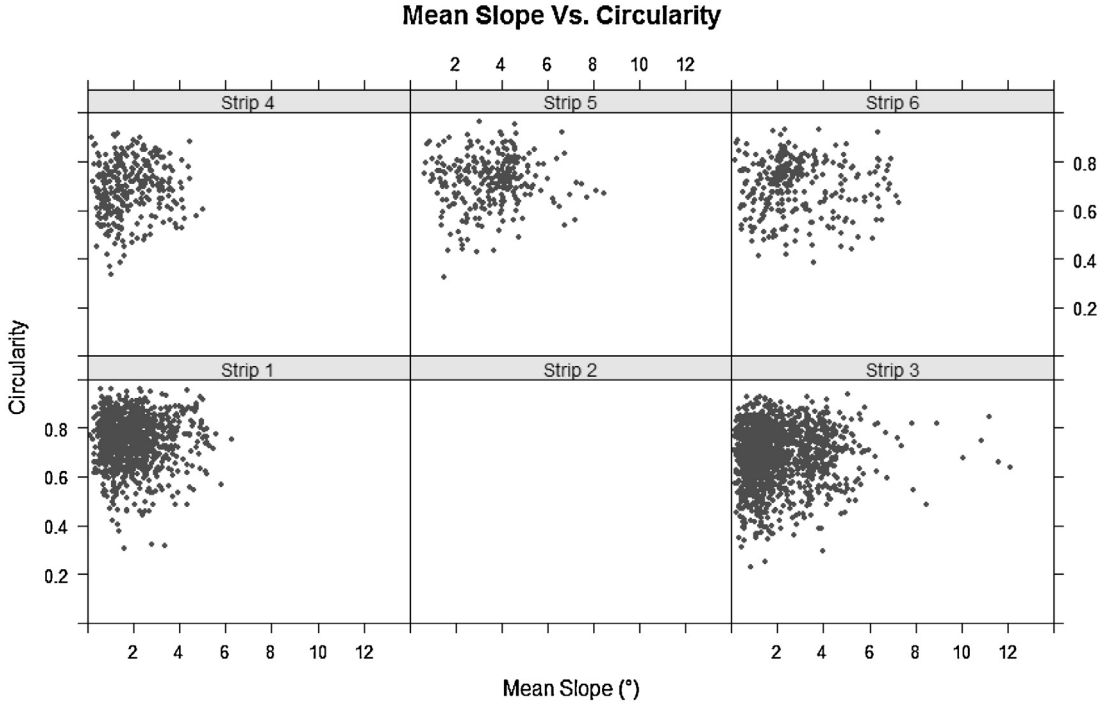

Fig. 20. Scatterplots displaying the relationship between the circularity of polygons and their mean slope. There is no suitable 3D data available for strip 2 and therefore no slope data.

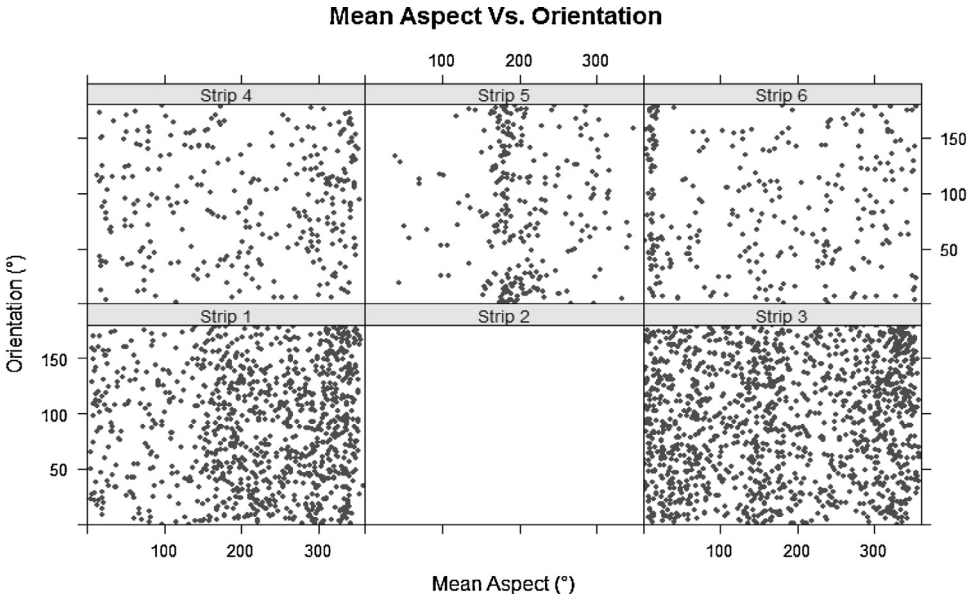

Fig. 21. Scatterplots displaying the relationship between the orientation of polygons and their mean aspect. There is no suitable 3D data available for strip 2 and therefore no orientation data.

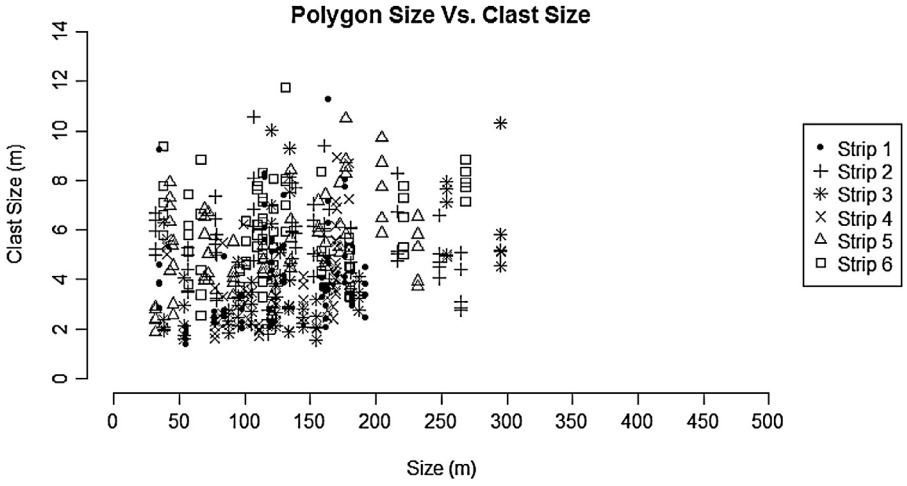

Fig. 22. Scatterplot displaying the relationship between polygon size and clast size.

and Mars (Barrett, 2014). The figure indicates that, although Lyot polygons are far larger, their circularity values are within the range of both sorted patterned ground and thermal contraction crack polygons. Sorted patterned ground values show a larger spread compared to the other polygon types and, in general, the mean values for circularity from Lyot are closer to the values indicated for thermal contraction crack polygons.

Next, we examine whether larger Lyot polygons contain larger marginal clasts, as might be expected for sorted periglacial patterned ground on Earth. Fig. 24 shows polygon size plotted against clast length. The datasets used as comparisons are all taken from sorted patterned ground. These include data from Iceland, Earth and around Lomonosov Crater, Mars (Barrett, 2014). Polygon data for known patterned ground displays a characteristic positive correlation where clast length increases with polygon size. The data for Lyot crater does not sit along this line, indicating that it does not follow this relationship. In fact, the clasts observed are similar in mean length to the larger measurements from Lomonosov Crater, although the polygon size values are far greater for the Lyot examples.

To test whether polygons of any formation mechanism are analogous in size and shape to those observed around Lyot crater exist on Earth or Mars, polygon size and lengths for our Lyot data and a variety of other datasets are compared (Table 5). Table 5 shows that the polygons found at Lyot crater are within the range of size values for large thermal contraction cracks from Utopia Planitia and the South Polar Layered Deposit on Mars, and also within the size ranges displayed by large desiccation polygons observed occasionally in playa environments on Earth. Sorted patterned grounds have size values that are far lower, as are the sizes of thermal contraction crack polygons on Earth. This might indicate that thermal contraction polygons on Mars are able to form with larger diameters than those on Earth, or that larger thermal contraction polygons are more poorly preserved on Earth.

The comparison of the Lyot clastic polygon data with data from other studies of polygonal features indicates that the Lyot crater polygons are comparable in size and circularity to some thermal contraction crack and desiccation polygons, but not to sorted clastic polygons. More specifically, they are similar in size and shape to thermal contraction crack polygons located on Mars, as the ter-

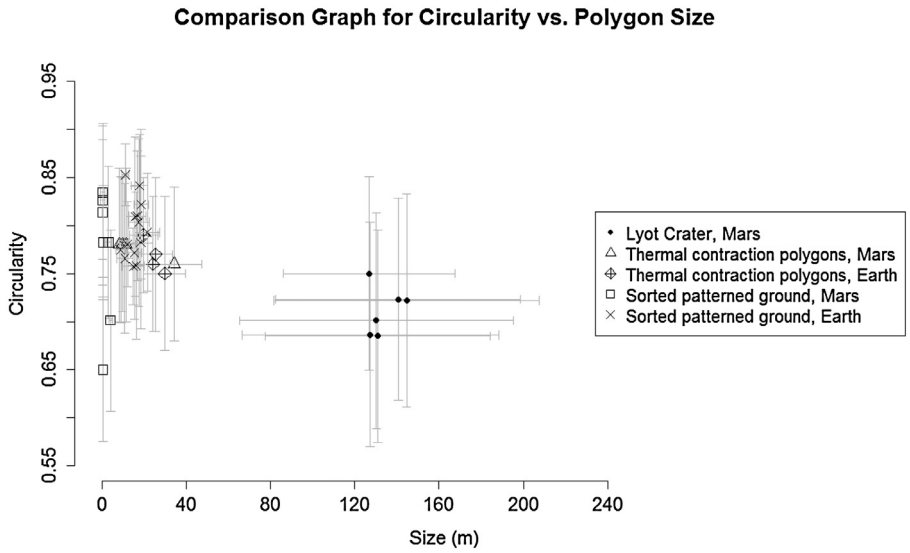

Fig. 23. Scatterplot of comparison data displaying the relationship between circularity and polygon size. The thermal contraction crack polygon values for Earth and Mars are taken from Ulrich et al. (2011). The sorted patterned ground values for Earth and Mars are adapted from Barrett (2014). For further information about these comparison data refer to Table 5. One standard deviation on the mean is used for the error bar values.

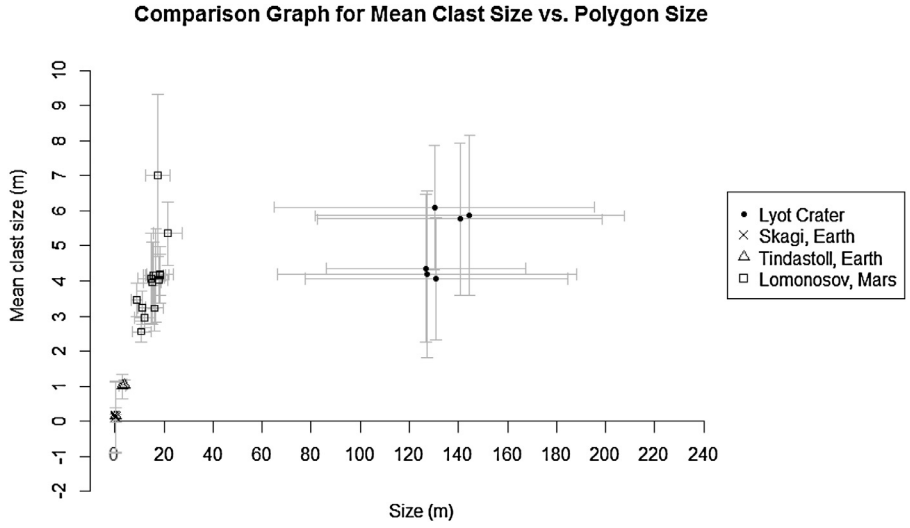

Fig. 24. Scatterplot of comparison data displaying the relationship between clast length and polygon size. Skagi, Tindastoll and Lomonosov values are adapted from Barrett (2014). One standard deviation is used for the error bar values.

restrial examples tend not to reach as large a size. Desiccation polygons can also occur at a similar scale to those which occur around Lyot, and the literature indicates that they possess a similar plan view to thermal contraction cracks. The plots analysed demonstrate that the Lyot forms have different morphological values than other sorted patterned ground: sorted patterned grounds are more circular than the polygons located around Lyot crater, although the spread of data could encompass those at Lyot, and they are far smaller in size. This could be a result of the sorted patterned ground data selected for use in this study, but we note that there are almost no published observations of sorted patterned ground with diameters greater than ~10–20 m. A further relationship, that between clast size and polygon size, also indicates that the Lyot polygons do not follow the typical "sorted patterned ground" relationship, with clasts too small and polygons too large.

6. Discussion

6.1. Comparison of the Lyot clastic polygons and periglacial sorted patterned ground

Clastic polygonal networks around Lyot crater morphologically resemble sorted patterned ground in that they have clastic material and low centres (Fig. 1B). However, their large size is unusual. Sorted patterned ground rarely contains polygons or circles greater than a few metres in diameter, although maximum diameters of around 10 metres have been observed on Earth (Washburn, 1956; Treml, 2010; Feuillet et al., 2012) and possible examples on Mars of around 23 to 25 metres in diameter have been observed (Balme et al., 2009; Barrett, 2014; Soare et al., 2016). The typical polygon found at Lyot crater is ~130 metres in diameter, more than 10 times the size of those found on Earth, and more than 5 times

Table 5
Comparison data displaying the average sizes and lengths for various polygons taken from the literature. Where an average value is not available a range has been used.

Location	Source	Polygon Type	Size (m)	SD	Length (m)	SD
Lyot crater, Mars	This study	To be determined	130.5	56.18	179.2	78.05
Skagi, Iceland, Earth	Barrett (2014)	Sorted patterned ground	0.3	0.02	0.3	1.02
Tindastoll, Iceland, Earth	Barrett (2014)	Sorted patterned ground	4	0.88	5	1.68
High Sudetes, Central Europe, Earth	Treml et al. (2010)	Sorted patterned ground			3.7	
Adventdalen, Svalbard, Earth	Ulrich et al. (2011)	Thermal contraction cracks	29.7	1.4	40.9	14.9
Dry Valley, Antarctic, Earth	Yoshikawa (2003)	Thermal contraction cracks	12.7			
Barrow, Alaska, Earth	Yoshikawa (2003)	Thermal contraction cracks	16.3			
Adventdalen, Svalbard, Earth	Yoshikawa (2003)	Thermal contraction cracks	18.5			
Pingo dal, East Greenland, Earth	Yoshikawa (2003)	Thermal contraction cracks	38.2			
Alvord Desert, Oregon, Earth	Neal et al. (1968)	Desiccation Polygons			15 - 30	
Guano Lake, Oregon, Earth	Neal et al. (1968)	Desiccation Polygons			> 100	
Pit-Taylor Reservoir, Nevada, Earth	Neal et al. (1968)	Desiccation Polygons			15 - 30	
Smoke Creek Desert, Nevada, Earth	Neal et al. (1968)	Desiccation Polygons			30 - 75	
Coal Valley, Nevada, Earth	Neal et al. (1968)	Desiccation Polygons			75 - 100	
Jakes Valley, Nevada, Earth	Neal et al. (1968)	Desiccation Polygons			> 100	
Elysium Planitia, Mars	Balme et al. (2009)	Possible sorted patterned ground			13.7	3.4
Northern plains, Mars	Gallagher et al. (2011)	Possible sorted patterned ground			13	
Lomonosov, Mars	Barrett (2014)	Possible sorted patterned ground	21.4	5.91	25.4	8.57
Utopia Planitia, Mars	Ulrich et al. (2011)	Possible thermal contraction cracks	34.3	12.8	46.2	16.9
Utopia Planitia, Mars	Yoshikawa (2003)	Possible thermal contraction cracks	123.9			
South Polar Layered Deposit, Mars	Yoshikawa (2003)	Possible thermal contraction cracks	137.7			
Athabasca Valles, Mars	Burr et al. (2005)	Possible thermal contraction cracks			~25	~10
Giant Polygons, Mars	Yoshikawa (2003)	Km-scale polygons	7236.6			

the size of the other examples found on Mars. This would indicate an exceptionally large sorting depth of between ~33 to 43 metres based on a polygon diameter to sorting depth ratio of 3 to 4 (Ballantyne and Harris, 1994; Treml et al., 2010). A sorting depth of this scale is far larger than any previously observed and seems unlikely. This indicates that the formation of these polygons through freeze-thaw cycling alone is questionable. It has been observed that large polygons can form by the amalgamation of smaller sorted polygons over time (Kessler and Werner, 2003). This could potentially be indicated by the discontinuous clastic lines observed in the large polygon interiors (Fig. 14). On the other hand, burial by mantling units, as opposed to the elimination of small polygons, is another possibility – and could suggest that polygon sizes are somewhat overestimated. However, even taking this internal partitioning into account, and noting that it is not seen in all of the observed polygons, it seems unlikely that the difference in size between the Lyot clastic polygons and previous observations of more typical sorted polygonal ground is due to observation of only the largest polygons in the network, while smaller, internal ones are somehow always buried.

Terrestrial observations also indicate that there is a relationship between polygon diameter and clast size, with a ratio ranging from 1:5 to 1:10 (Goldthwaite, 1976). This positive correlation is not observed in the case of the clasts demarcating Lyot polygons. Furthermore, according to the ratio provided by Goldthwait (1976), the clasts in the Lyot polygons should be between 13 and 26 metres in diameter, but even the largest clasts observed around Lyot polygons are smaller than this lower limit (Table 1). It should also be noted that there is no evidence of the imbrication of clasts, which can occur as a result of frost sorting processes (Dahl, 1966; Kessler and Werner, 2003; French, 2007; Soare et al., 2016). Also, the observations of double lines of clasts, and of clasts that appear to have formed from the fracture of larger, elongate ridges of material do not match a periglacial sorting model (Fig. 15).

Finally, periglacial sorted patterned ground has a distinctive relationship with topography in which geometric forms change from polygons on slopes of 2 to 4°, to ellipses on slopes of 3 to 6°, and finally to stripes on slopes of 4 to 11° (Goldthwait, 1976). Therefore it is expected that sorted patterned ground on Mars will behave in a similar way, and that larger slopes will lead to a lower value for circularity indicating elongation. Such a relationship has been observed at other locations on the surface of Mars (e.g. Gallagher et al., 2011). Although a qualitative relationship between topography and the polygons is indicated from observations, there is no positive correlation between circularity and slope, and high circularity polygons have been recorded on slopes as large as 12° Also, no clastic stripes have been observed in this study.

Overall, the morphometric analysis and qualitative observations do not support the hypothesis that freeze-thaw sorting processes are responsible for formation of the clastic polygonal features around Lyot. Both Martian and terrestrial data indicate that there should be a stronger relationship between clast size and polygon diameter, and between polygon form and underlying slope and aspect than is observed (e.g. Goldthwait, 1976; Gallagher et al., 2011; Barrett, 2014). It should be noted that little quantitative data describing the relationship between polygon elongation and slope angle is currently available on Mars, although this relationship has been observed qualitatively. Similarly, there is also little comparison data available quantifying the relationship between clast size and polygon diameter on Mars. Nevertheless, the combined observations and measurements and their comparison with terrestrial and martian datasets suggest that a periglacial sorting origin is not the best working hypothesis to explain the Lyot clastic polygons.

6.2. Comparison of Lyot clastic polygons and thermal contraction crack polygons

Thermal contraction crack polygons vary in morphology and size depending upon subsurface properties and the environment in which they form. The Lyot crater study area contains landforms and landscapes indicative of a cold environment with brief, possibly climate-driven, periods of fluvial activity. Fractures would be affected by topography and this could explain the oriented polygonal features observed around topographic features. This suggests that the thermal contraction of ice-cemented soils could be a potential mechanism to form patterned ground in this area – especially if a mechanism exists that could allow a “wedge-type” polygon to evolve into a “clast-bounded” polygon. The formation of these wedge-type polygons around Lyot is discussed here, and their morphology and morphometric properties are compared to those of the Lyot clastic polygons. We discuss whether thermal

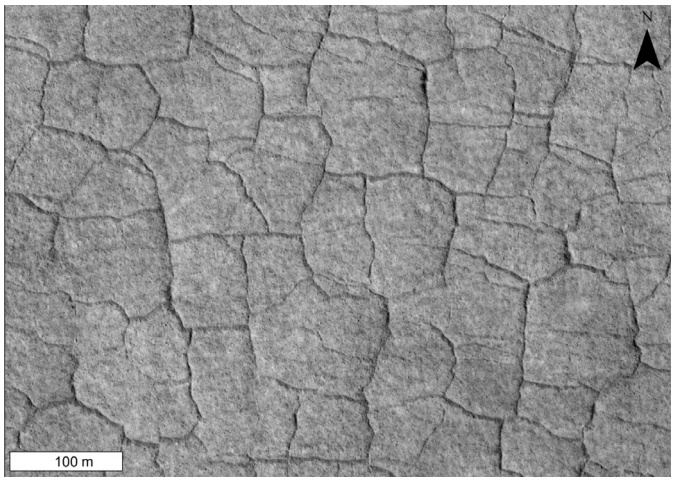

Fig. 25. HiRISE (PSP_002070_2250) image of possible thermal contraction crack polygons located in Utopia Planitia (45°N, 88°E). The polygons have somewhat similar sizes and morphologies to the network shape seen in the polygons located around Lyot crater. The terrain in this area contains scalloped depressions (Séjourné et al., 2011) and a surficial layer of small clastic material. Image credit: NASA/JPL/University of Arizona.

contraction features could evolve to form the clast-bounded polygons observed later.

Typical diameters for terrestrial ice-wedge polygons range from 10 to 40 metres with maximum diameters of over 100 metres (Washburn, 1956; Black, 1976; Washburn, 1980; Maloof et al., 2002). On Mars, possible thermal contraction polygons of a similar size to the clastic polygons around Lyot crater, with diameters ranging from 30 to 170 metres (Fig. 25; Yoshikawa, 2003; Lefort et al., 2009), have been observed in Utopia Planitia. Hence, there is evidence that thermal contraction cracking on Mars can produce polygonal ground of the same spatial scale as the Lyot clastic polygons – although a simple thermal contraction crack mechanism would not explain their clastic boundaries. It has been also observed that thermal contraction polygons potentially subdivide into smaller polygons over time (Greene, 1963; Black, 1976), this might be analogous to the internal partitioning observed inside some of the larger Lyot clastic polygons (Fig. 14).

Taking each subtype separately, sand-wedge and composite-wedge polygons appear more likely to produce the gross polygon morphology and scale observed at Lyot. Sublimation polygons are rare on Earth, and require underlying massive ice or excess ice (as opposed to ice-rich sediments or soils) directly beneath the layer in which the polygons form. While this might have been the case here, we note that sublimation polygons are usually both smaller than wedge type polygons, and form broader dome-like features with more poorly defined marginal troughs. Hence we think that they are less likely to be good analogues for the Lyot clastic network patterns than wedge-type polygons.

Sand-wedge and composite-wedge polygons can form low-centred polygons as a result of the forcing of material upwards on either side of the initial fracture. This can lead to the realigning of clasts and the production of a double rimmed appearance (Black, 1976; French, 2007), as is seen at Lyot (Fig. 15). Although ice-wedge polygons can also produce this surface morphology, one might expect ice exposed to the Martian surface environment to sublime, leading to the formation of pits or other signs of collapse and eventually a high-centred appearance, as described for other parts of Mars (Levy et al., 2011), unless it were shielded from the surface by a layer of desiccated material (e.g., Lefort et al., 2009). Ice-wedge polygons also indicate the presence of a more humid environment, to allow for the growth of an ice-wedge, whereas sand-wedge polygons occur in a more arid environment where ice occurs in pore spaces within the sediment (Pewe, 1959; Black, 1976; French, 2007). Although Lyot has experienced periods of fluvial activity, indicating the past presence of water (Dickson et al., 2009; Fassett et al., 2010; Hobley et al., 2014), and ice-rich material is located nearby in the form of mantling units, it might be expected that ice deposited in the fractures would sublime without sufficient cover, leading to the formation of troughs. It appears more likely that wind-blown sediment might infill exposed fractures resulting in a sand-wedge. Alternatively, obliquity-driven changes in climate (Laskar et al., 2004) might have resulted in variations in humidity and pressure leading to composite-wedge or ice-wedge polygon formation.

The polygonal networks around Lyot possess similar intersection angles to terrestrial mature thermal contraction polygonal networks, tending towards 120° with, on average, 5-sided polygons (French, 2007). The Utopia Planitia polygons also tend towards equiangular intersections of ~120° (Lefort et al., 2009), although they appear more regular than the Lyot networks (Fig. 25). Thus they are somewhat similar in both polygon size and network shape to the Lyot polygons.

In both terrestrial thermal contraction polygons, and the polygons present in Utopia Planitia, troughs bound the polygons. Troughs are not visible around the clastic polygons at Lyot.

Hence, while it can be shown that there are examples of Martian thermal contraction polygons similar in size and overall shape to the polygonal networks seen in Lyot, and that the action of either a sand-wedge or composite-wedge polygon formation mechanism appears plausible in this current environment, the clastic appearance of the Lyot polygons provides a very clear contrast to the usual morphology of thermal contraction polygons on Earth or elsewhere on Mars. It is possible that the gravitational slumping of overlying clastic material into the fractures could be responsible for allowing a clastic-bounded polygon to evolve from a thermal contraction crack polygon, but in the Lyot study area there is no relationship between boulder fields and polygons, there is no evidence for troughs at the polygon margins, and there is generally an absence of boulders within the polygons between the clastic margins: the clasts seem too well-confined to the polygon boundaries to have formed by gravitational slumping from what was originally a boulder-rich terrain.

We therefore provide another possible, but somewhat speculative, alternative formation hypothesis: if a thermal contraction crack network formed, and was then infilled by later materials, then this infilling material could become indurated or cemented within the fractures. This material could then be revealed in positive relief if there were general downwearing of the landscape, perhaps due to climatic changes and enhanced aeolian erosion. These lines of inverted, erosion resistant fracture-fill could then themselves degrade to produce clasts. This explanation is consistent with some of the detailed observations of the Lyot polygons, such as linear clasts, and double lines of clasts that might have formed from material forming on either side of a centrally fractured sand-wedge or composite-wedge. Furthermore, it is also broadly in keeping with the overall polygon size and network shape.

6.3. Comparison of Lyot clastic polygons and desiccation polygons

Having compared the Lyot clastic polygons to thermal contraction fracture polygons, we now consider whether they could have formed as, or evolved from, desiccation polygons. Desiccation polygons have been observed at a wide range of scales on Earth: although they rarely exceed 1 metre in diameter, rare examples of up to 300 metres across exist (Neal et al., 1968). This sets them within the size range of the clastic polygons around Lyot crater. Therefore,

a process similar to that suggested for thermal contraction cracks above, by which infill of fractures, induration/cementation of fill, and inversion of the fill forms clastic polygons, might be invoked.

However, to produce desiccation polygons of this scale, the stressed region would need to be thick to produce deep fractures, and the environment would need to have first been very humid, then have experienced a period of intense aridity combined with lowering of the ground-water level (Neal et al., 1968; El Maarry et al., 2012). Desiccation polygons are generally associated with remnant lacustrine deposits in a playa environment (Neal et al., 1968; Loope and Haverland, 1988; El Maarry et al., 2010; El Maarry et al., 2012; El Maarry et al., 2014). This indicates that sustained fluvial activity would be necessary to form large desiccation polygons. On Mars, such a body of water could be a crater lake sustained by a hydrothermal system, as thermal energy would need to be provided to sustain a body of water on the surface of Mars (El Maarry et al., 2010; El Maarry et al., 2012; El Maarry et al., 2014). The clastic polygonal features around Lyot appear to be geologically recent and so must have formed far later than the impact event which formed the crater, so any hydrothermal activity, or remnant heat from the impact would have long-since dissipated.

Although there is geomorphological evidence consistent with the presence of fluvial activity on the inner ejecta blanket, there is no evidence of standing bodies of water occurring on the outer ejecta blanket of Lyot, and the clastic polygons occur on areas of higher topography rather than depressions where standing water would be present. Given the geographical setting, and the fact that the clastic polygons appear to form on the upper parts of hummocks, it seems unlikely that desiccation cracking is the origin of the clastic polygonal ground around Lyot.

6.4. Other mechanisms

Polygonal grounds of somewhat similar network morphology to the clastic polygons located around Lyot crater include the thermal contraction of cooling lava (e.g. Peck and Minakami, 1968), the subaqueous contraction of sedimentary gel, termed syneresis (e.g. Dewhurst et al., 1999), the formation of polygonal fault systems via the intersection of a series of normal faults within marine basins (e.g. Tewksbury et al., 2014), and the polygonal weathering of sedimentary rocks (e.g. Williams and Robinson, 1989). We now briefly consider whether any of these mechanisms could have created, or evolved to form, the Lyot clastic polygons.

The thermal contraction of cooling lava can produce polygons up to decametres in size (Peck and Minakami, 1968; Grossenbacher and McDuffie, 1995; Hetényi et al., 2012). These polygons, also referred to as columnar joints, have a high centred appearance and tend towards a hexagonal shape (Toramaru and Matsumoto, 2004). Polygons of this type are far smaller than those observed around Lyot crater and possess a different typical morphology. There are also no lava-like flows associated with Lyot polygons, no possible sources of lava visible, and the distribution on top of small hummocks, and around the crater, cannot be explained by this polygon type. Thus the thermal contraction of lava can be eliminated as a potential hypothesis.

Syneresis is a process that occurs in fine-grained sediments such as mudstones within a subaqueous environment (Pratt, 1998; Coker et al., 2007). Polygons attributed to syneresis vary in diameter from crack patterns of centimetres in scale (Pratt, 1998) to polygonal fault systems of decametres to kilometres in scale (Dewhurst et al., 1999; Coker et al., 2007; Moscardelli et al., 2012). Typically, such polygons are found in slope or basin-floor depositional settings (Moscardelli et al., 2012). Lyot polygons are low-centred, as opposed to high-centred, and occur at a different range of scales to that typical of syneresis polygons. There is also a lack of evidence indicating a subaqueous basin environment, and because of this it is expected that syneresis would be unlikely to have occurred. Thus, it is suggested that a hypothesis involving syneresis can be eliminated.

Syneresis is also the primary mechanism suggested for the formation of polygonal fault systems formed via the intersection of a series of normal faults. Such fault systems occur in deep marine basin environments, with typical polygon diameters of kilometres (Dewhurst et al., 1999; Watterson et al., 2000; Moscardelli et al., 2012; Tewksbury et al., 2014). Polygons around Lyot crater average 130 metres in size, which is significantly lower than polygons formed by polygonal fault systems. There is also a lack of evidence for a deep marine environment around Lyot crater at this time. Due to these factors it is suggested that polygonal faulting can be eliminated as a hypothesis.

Polygonal weathering occurs on the exposed surfaces of boulders and rock outcrops composed of massive sandstone (Williams and Robinson, 1989). The cracks are pentagonal to hexagonal in shape and can be flat, concave or convex (Williams and Robinson, 1989). Most such polygons are between 10 and 20 cm in diameter (Williams and Robinson, 1989), with maximum polygon sizes recorded of metres in scale (Chan et al., 2008). Small polygons can be contained within large polygons giving a nested appearance (Chan et al., 2008). The polygons around Lyot crater are typically over 100 times larger than the largest polygonal features formed by weathering on Earth. The Lyot polygons also do not display a nested appearance, although small nested polygons could perhaps be obscured by later mantling deposits. It is therefore suggested that the polygonal weathering of sedimentary rocks can also be eliminated as a possible formation hypothesis for the Lyot clastic polygons.

6.5. Possible formation mechanisms for the clastic polygons around Lyot crater

Based upon the previous discussion it is suggested that thermal contraction crack polygons, in particular sand-wedge or composite-wedge polygons, provide the best morphometric and morphological analogue to the polygonal network patterns of the Lyot clastic polygons. On Mars, the best size and shape analogue is found in Utopia Planitia, proposed to have formed through thermal contraction cracking (Yoshikawa, 2003; Lefort et al., 2009).

However, thermal contraction cracking does not explain the concentration of clasts at the boundaries of the polygon margins. There are a number of suggested mechanisms by which clastic material can concentrate in thermal contraction polygon boundaries. These include freeze-thaw cryoturbation, as in sorted patterned ground, gravitational slumping, and CO_2 frost ratcheting, whereby boulders become locked in a layer of CO_2 ice and are forced outwards as thermal contraction and expansion occurs (Orloff et al., 2013). The size of the clasts found in the Lyot polygons are almost certainly too large to have been moved via a freeze-thaw or CO_2 ratcheting process, so we reject this as a mechanism.

We now consider gravitational slumping of a pre-existing population of clasts. This might occur if clasts were ejected during the Lyot impact event and later concentrated into the thermal contraction fractures by gravity (e.g., Levy et al., 2010). In this case we would expect there to be a pre-existing boulder field of large clastic material around the polygonal features, as clasts the size of those found at Lyot are unlikely to have travelled far before slumping into the fractures. Taking this into consideration we would expect: (i) evidence of an association of the polygonal networks with boulder fields and (ii) for clasts of a similar morphology to those observed within the polygon margins to be present away from these margins, within the polygons centres. These relationships have not been observed: the large boulder fields are located away from the clastic polygonal networks, and, where a small boulder-

rich area is present, we find a cleared margin between the edge of the clastic network and boulder-rich area (Fig. 13). Large angular clasts are not observed located away from polygon margins, only smaller, more circular clasts are seen (Fig. 15). Also, gravitational slumping does not account for the large ridge like clasts that have been observed in distinctive double rim patterns (Fig. 15).

Another indicator of gravitational slumping is for the clastic material to be associated with fractures or located within troughs (Levy et al., 2010; Barrett et al., 2017). We have seen no evidence of either fractures or troughs associated with the clastic material, polygonal margins are high standing and clasts do not appear to be located within depressions (Fig. 16). It is also not certain how angular boulders of the scale of those observed at Lyot would be moved via a process of gravitational slumping as the slopes seen in this study are low, with a maximum angle of 12° (Table 2). Finally, a recent study (Barrett et al., 2017) has indicated that fracture control mechanisms (such as gravitational slumping) of clasts into patterns could largely be a result of chance, and that fractures did not seem to substantially influence the arrangement of clasts at most sites where both clasts and fractures are present. Therefore, we reject the idea that gravitational slumping of a pre-existing population of boulders into thermal contraction cracks was the process by which the clasts forming the Lyot polygons were concentrated.

We therefore return to the mechanism suggested previously: the clasts are the result of the infilling of pre-existing polygonal fractures with wind-blown sediments and/or ice, followed by cementation or induration of this fill, and then differential erosion, which exposes the network. Finally, weathering the indurated fill material formed the pattern of blocks seen today. In this case, the network is the trace of the exposed sand-wedge or composite-wedge network itself. This mechanism explains many of the observations and morphological features of the polygons, although the large size of the polygons is still difficult to fully explain, given that many are larger than even the thermal contraction crack polygons identified in Utopia Planitia (Yoshikawa, 2003; Lefort et al., 2009). Furthermore, the suggested mechanism in which fill material is indurated, then fractured, to form the clasts does not appear to have been observed elsewhere on the surface of Mars or on Earth; terrestrial clastic polygons are generally the result of gravitational slumping or freeze-thaw processes. This indicates that either the method for clast formation is unique, or the environment must have been unique such that a previously observed mechanism acted on such a scale. Furthermore, there is no clear reason why fracture fill should become indurated or cemented here, but not in other locations on Mars. Further investigation is clearly required to more fully understand how these enigmatic features have formed.

6.6. The spatial distribution of clastic polygons and "primary" formation hypotheses

A key characteristic of the Lyot polygons is their spatial distribution: their specific location on the Lyot ejecta blanket, at a narrow range of radial distances from the crater rim, indicates a genetic link with the crater itself. It seems unlikely that the polygons formed in this pattern by chance. This indicates either that this region of the ejecta hosts a unique material type, and/or a unique process has acted on the materials here. Given the radial distribution of the polygons, it seems the explanation must lie with the composition of the ejecta – and hence with the type of material ejected from a particular depth during the impact event. For example, if a vertically constrained, sub-surface layer of a specific composition was penetrated by the Lyot-forming impact, ejecta from this layer might be deposited in a radial band at a certain distance from the crater. It might be speculated that a water-rich layer could thus result in a region of ejecta with high water or ice content being emplaced which, in turn, could be susceptible to certain processes that led to the unique polygonal morphologies seen here today.

Alternatively, the spatial link between the crater and clastic polygons could suggest a completely different formation hypothesis to those proposed above: namely that the polygons are primary, structural features picked out by erosion. In this scenario, and like many impact events (Rodríguez et al., 2005), the formation of Lyot resulted in extensive fracturing of the surface. Radial and concentric fault systems are often found around impact craters (Rodríguez et al., 2005). It is possible that such a fault system could then have been exploited by hydrothermal fluids, resulting in the formation of vein networks. Later erosion might result in the exposure of these veins as a high relief feature. An issue for this hypothesis, however, is that fracture networks around impact craters do not possess an organised polygonal appearance. Furthermore, the fracture network would be expected to be more continuous around the crater rather than within only a specific area of the outer ejecta blanket, and it also seems unlikely that such fractures would penetrate through the outer, poorly consolidated ejecta to the surface.

Another "primary" mechanism for the formation of polygonal fractures or patterns in the ejecta of Lyot is that of fracturing of impact melt ponds, as seen in several craters on the Moon and Mercury (e.g. Xiao et al., 2014). While some examples of such fracturing are superficially similar to the patterns seen at Lyot, they are generally much larger (>100 s of metres in diameter) and also form in well-defined, low standing melt ponds. This is not the case in Lyot, as the polygons appear to be forming on the tops and margins of hummocks in the outer ejecta. Thus, while primary formation mechanisms might be invoked, we think they are unlikely, and that the most likely formation mechanisms for the creation of the Lyot clastic polygons are secondary, and occurred after the outer ejecta was emplaced. We therefore suggest that the relationship between the distribution of the polygons and the site of the Lyot crater is due to the composition of the outer ejecta material as opposed to a structural relation.

7. Conclusion and further work

Enigmatic clastic polygonal networks located around Lyot crater were studied using morphometric analysis and qualitative morphological observations to provide information by which a possible formation mechanism might be inferred. Amongst the large population of observed polygons on Mars, the Lyot polygons are unique on Mars in that they have clastic margins and average diameters of 130 metres, far larger than clastic polygons observed on Mars or Earth. The polygons are generally five or six sided with average intersection angles of 120° Polygons tend toward equidimensional rather than elongate forms, with geometric shape largely independent of slope or aspect. The clastic blocks which compose the polygon edges are angular, with an average maximum clast size of 5 metres. Clast size does not increase with polygon size. These results taken together indicate that polygons are unlikely to be the result of freeze-thaw processes.

The morphometric data we collected were compared to various terrestrial and Martian polygon datasets to observe any trends or associations. Quantitative analysis using high-resolution remote-sensing data, based upon the method of Ulrich et al. (2011), and comparison to existing polygon datasets demonstrates that the Lyot polygons are comparable in size and shape to some desiccation polygonal fracture networks on Earth and some thermal contraction polygon networks on Mars. Qualitative observations indicate the Lyot polygons are similar to large-scale sorted patterned ground or thermal contraction cracks, but with important differences, such as their very large diameters, their large clast size in-

dependent of polygon diameter, their double-rimmed clastic borders and their elongated border clasts. Based upon these data, and a literature review of other geological polygonal features, thermal contraction cracks are proposed as the most likely mechanism by which the initial Lyot fracture networks formed.

Quantitative analysis of the morphometric data, and careful qualitative analysis of the morphology and context of the Lyot clastic polygons, seems to rule out simple gravitational slumping of pre-existing boulders into fractures as the mechanism by which initially negative relief polygon boundaries became erosion-resistant, positive relief boundaries.

We describe an alternative mechanism in which thermal contraction cracks are infilled with wind-blown sediment, and potentially ice, which forms resistant-fill material. The polygons are then buried by later mantle deposits which are eroded/ablated away leading to exhumation, fracturing of the resistant fill and the formation of angular clastic borders. We note that this mechanism explains many of the characteristics of the Lyot clastic polygons, but that the induration/cementation mechanism remains to be described.

The distribution of the clastic polygonal networks indicates a relationship between the clastic polygonal networks and the composition of the outer ejecta material. However, several lines of morphological and contextual evidence argue against a primary, structural or impact-melt derived mechanism for the formation of the Lyot clastic patterned ground.

This suggests that the formation of clastic polygons is related to the material exhumed from a specific depth during the Lyot crater impact event. Such material could have been ice-rich and susceptible to certain processes leading to the formation of the exceptionally large clastic polygons observed. Thus, further work will involve the numerical modelling of this impact event to identify the depth from which such material might be exhumed, and whether this is related to the depth of the Martian cryosphere in this area.

We conclude that, although large amounts of data have been gathered that describe the setting, morphometry and morphology of these enigmatic clastic polygons, and many formation hypotheses described and tested, no single hypothesis can satisfactorily explain their origin. Our favoured hypothesis is that the polygons formed by inversion of polygonal thermal contraction crack networks by infill, cementation/induration and differential erosion.

Acknowledgements

LMB is funded by the Science and Technology Facilities Council of the UK under STFC grant ST/M503691/1. SJC acknowledges support from the French Space Agency CNES for her HiRISE work. We would like to thank Jay Dickson and Ernst Hauber for their excellent reviews that have helped to improve this paper.

References

Ballantyne, C.K., Harris, C., 1994. The Periglaciation of Great Britain. Cambridge University Press, Cambridge, United Kingdom.

Balme, M.R., Gallagher, C.J., Page, D.P., Murray, J.B., Muller, J.–P., 2009. Sorted stone circles in Elysium Planitia, Mars: implications for recent martian climate. Icarus 200 (1), 30–38.

Balme, M.R., Gallagher, C.J., Hauber, E., 2013. Morphological evidence for geologically young thaw of ice on Mars: a review of recent studies using high-resolution imaging data. Prog. Phys. Geog. 37 (3), 289–324.

Barrett, A., 2014. An investigation of potential periglacial landforms on the northern plains of Mars: An integrated field, laboratory and remote sensing study Doctoral thesis. Open University, Milton Keynes, United Kingdom.

Barrett, A., Balme, M.R., Patel, R.P., Hagermann, A., 2017. Clastic patterned ground in Lomonosov crater, Mars: examining fracture controlled formation mechanisms. Icarus 295, 125–139.

Bertran, P., Klaric, L., Lenoble, A., Masson, B., Vallin, L., 2010. The impact of periglacial processes on Palaeolithic sites: the case of sorted patterned grounds. Quat. Int. 214 (1-2), 17–29.

Black, R.F., 1976. Periglacial features indicative of permafrost: ice and soil wedges. Quat. Res. 6 (1), 3–26.

Burr, D.M., Soare, R.J., Tseung, J.M.W.B., Emery, J.P., 2005. Young (late Amazonian), near-surface, ground ice features near the equator, Athabasca Valles, Mars. Icarus 178, 56–73.

Chan, M.A., Yonkee, W.A., Netoff, D.I., Seiler, W.M., Ford, R.L., 2008. Polygonal cracks in bedrock on Earth and Mars: implications for weathering. Icarus 194 (1), 65–71.

Coker, M.O., Bhattacharya, J.P., Marfurt, K.J., 2007. Fracture patterns within mudstones on the flanks of a salt dome: Syneresis or slumping? Gulf Coast Assoc. Geolog. Soc. Trans. 57, 125–137.

Dahl, R., 1966. Block fields, weathering pits and tor-like forms in the Narvik Mountains, Nordland, Norway. Geogr. Ann., Ser. A 48 (2), 55–85.

Dewhurst, D.N., Cartwright, J.A., Lonergan, L., 1999. The development of polygonal fault systems by syneresis of colloidal sediments. Mar. Pet. Geol. 16 (8), 793–810.

Dickson, J.L., Fassett, C.I., Head, J.W., 2009. Amazonian-aged fluvial valley systems in a climatic microenvironment on Mars: Melting of ice deposits on the interior of Lyot crater. Geophys. Res. Lett. 36 (8). doi:10.1029/2009GL037472.

El Maarry, M.R., Markiewicz, W.J., Mellon, M.T., Goetz, W., Dohm, J.M., 2010. Crater floor polygons: desiccation patterns of ancient lakes on Mars? J. Geophys. Res. 115 (E10). doi:10.1029/2010JE003609.

El Maarry, M.R., Kodikara, J., Wijessoriya, S., Markiewicz, W.J., Thomas, N., 2012. Desiccation mechanism for formation of giant polygons on Earth and intermediate–sized polygons on Mars: results from a pre-fracture model. Earth Planet. Sci. Lett. 323 – 324, 19–26.

El Maarry, M.R., Watters, W., McKeown, N.K., Carter, J., Noe Dobrea, E., Bishop, J.L., Pommerol, A., Thomas, N., 2014. Potential desiccation cracks on Mars: a synthesis from modelling, analogue-field studies, and global observations. Icarus 241, 248–268.

Fassett, C.I., Dickson, J.L., Head, J.W., Levy, J.S., Marchant, D.R., 2010. Supraglacial and proglacial valleys on Amazonian Mars. Icarus 208, 86–100.

Feuillet, T., Mercier, D., Decaulne, A., Cossart, E., 2012. Classification of sorted patterned ground areas based on their environmental characteristics (Skagafjörður, Northern Iceland). Geomorphology 139 – 140, 577–587.

French, H.M., 2007. The Periglacial Environment, 3rd ed. John Wiley, Chichester, UK.

Gallagher, C., Balme, M.R., Conway, S.J., Grindrod, P.M., 2011. Sorted clastic stripes, lobes and associated gullies in high-latitude craters on Mars: Landforms indicative of very recent, polycyclic ground-ice thaw and liquid flows. Icarus 211 (1), 458–471.

Goldthwait, R.P., 1976. Frost sorted patterned ground: a review. Quat. Res. 6, 27–35.

Greeley, R. and Guest, J. 1987. Geologic map of the eastern equatorial region of Mars. U.S. Geological Survey Map I-1802-B.

Grab, S., 2002. Characteristics and palaeoenvironmental significance of relict sorted patterned ground, Drakensberg plateau, southern Africa. Quat. Sci. Rev. 21, 1729–1744.

Greene, G.W., 1963. Contraction theory of ice-wedge polygons: a qualitative discussion. In: Permafrost international conference: proceedings, pp. 11–15.

Groisman, A., Kaplan, E., 1994. An experimental study of cracking induced by desiccation. Europhys. Lett. 25 (6), 415–420.

Grossenbacher, K.A., McDuffie, S.M., 1995. Conductive cooling of lava: columnar joint diameter and stria width as functions of cooling rate and thermal gradient. J. Volcanol. Geotherm. Res. 69 (1-2), 95–103.

Haltigin, T.W., Pollard, W.H., Dutilleul, P., Osinski, G.R., 2012. Geometric evolution of polygonal terrain networks in the Canadian high arctic: evidence of increasing regularity over time. 2012. Permafr. Periglac. Process. 23 (3), 178–186.

Harrison, T.N., Malin, M.C., Edget, K.S., Shean, D.E., Kennedy, M.R., Lipkaman, L.J., Cantor, B.A., Posiolova, L.V., 2010. Impact-induced overland fluid flow and channelized erosion at Lyot crater, Mars. Geophys. Res. Lett. 37 (21). doi:10.1029/2010GL045074.

Hetényi, G., Taisne, B., Garel, F., Médard, E., Basshard, S., Mattsson, B.H., 2012. Scales of columnar jointing in igneous rocks: field measurements and controlling factors. Bull. Volcanol. 74 (2), 457–482.

Hobley, D.E.J., Howard, A.D., Moore, J.M., 2014. Fresh shallow valleys in the Martian midlatitudes as features formed by meltwater flow beneath ice. J. Geophys. Res.: Planets 119 (1), 128–153.

Kessler, M.A., Werner, B.T., 2003. Self-organization of sorted patterned ground. Science 299, 380–383.

Kirk, R.L., Howington-Kraus, E., Rosiek, M.R., Anderson, J.A., Archinal, B.A., Becker, K.J., Cook, D.A., Galuszka, D.M., Geissler, P.E., Hare, T.M., Holmberg, I.M., Keszthelyi, L.P., Redding, B.L., Delamere, W.A., Gallagher, D., Chapel, J.D., Eliason, E.M., King, R., McEwen, A.S., 2008. Ultrahigh resolution topographic mapping of Mars with MRO HiRISE stereo images: meter-scale slopes of candidate Phoenix landing sites. J. Geophys. Res. 113 (E00A24). doi:10.1029/2007JE003000.

Lachenbruch, A.H., 1962. Mechanics of thermal contraction cracks and ice-wedge polygons in permafrost. Geolog. Soc. Am. Spec. Pap. 70, 1–66.

Laskar, J., Correia, A.C.M., Gastineau, M., Joutel, F., Levrard, B., Robutel, P., 2004. Long term evolution and chaotic diffusion of the insolation quantities of Mars. Icarus 170 (2), 343–364.

Leffingwell, E.deK., 1915. Ground-ice wedges: the dominant form of ground-ice on the north coast of Alaska. J. Geol. 23 (7), 635–654.

Lefort, A., Russell, P.S., Thomas, N., McEwen, A.S., Dundas, C.M., Kirk, R.L., 2009. Observations of periglacial landforms in Utopia Planitia with the high resolution imaging science experiment (HiRISE). J. Geophys. Res. 114 (E04005). doi:10.1029/2008JE003264.

Levy, J.S., Marchant, D.R., Head, J.W., 2006. Distribution and origin of patterned ground on Mullins Valley debris-covered glacier, Antarctica: the roles of ice flow and sublimation. Antarct. Sci. 18 (3). doi:10.1017/S0954102006000435.

Levy, J.S., Head, J.W., Marchant, D.R., Kowalewski, D.E., 2008a. Identification of sublimation-type thermal contraction crack polygons at the proposed NASA Phoenix landing site: implications for substrate properties and climate-driven morphological evolution. Geophys. Res. Lett. 35 (4). doi:10.1029/2007GL032813.
Levy, J.S., Head, J.W., Marchant, D.R., 2008b. The role of thermal contraction crack polygons in cold-desert fluvial systems. Antarct. Sci. 20 (6), 565–579.
Levy, J.S., Marchant, D.R., Head, J.W., 2010. Thermal contraction crack polygons on Mars: a synthesis from HiRISE, Phoenix and terrestrial analog studies. Icarus 206, 229–252.
Levy, J.S., Head, J.W., Marchant, D.R., 2011. Gullies, polygons and mantles in Martian permafrost environments: cold desert landforms and sedimentary processes during recent Martian geological history. Geol. Soc., London, Spec. Publ. 354, 167–182.
Loope, D.B., Haverland, Z.E., 1988. Giant desiccation fissures filled with calcareous eolian sand, Hermosa Formation (Pennsylvanian), southeastern Utah. Sediment. Geol. 56, 403–413.
MacKay, J.R., 1984. The frost heave of stones in the active layer above permafrost with downward and upward freezing. Arct. Alp. Res. 16 (4), 439–446.
Malin, M.C., Bell, J.F., Cantor, B.A., Caplinger, M.A., Calvin, W.M., Clancy, R.T., Edgett, K.S., Edwards, L., Haberle, R.M., James, P.B., Lee, S.W., Ravine, M.A, Thomas, P.C., Wolff, M.J., 2007. Context Camera Investigation on board the Mars Reconnaissance Orbiter. J. Geophys. Res. 112 (E05S04). doi:10.1029/2006JE002808.
Maloof, A.C., Kellogg, J.B., Anders, A.M., 2002. Neoproterozoic sand wedges: crack formation in frozen soils under diurnal forcing during a snowball Earth. Earth Planet. Sci. Lett. 204, 1–15.
Mangold, N., 2005. High latitude patterned grounds on Mars: classification, distribution and climatic control. Icarus 174, 336–359.
Marchant, D.R., Lewis, A.R., Phillips, W.M., Moore, E.J., Souchez, R.A., Denton, G.H., Sugden, D.E., Potter Jr., N., Landis, G.P., 2002. Formation of patterned ground and sublimation till over Miocene glacier ice in Beacon Valley, southern Victoria Land, Antarctica. Geol. Soc. Am. Bull. 114 (6), 718–730.
Marchant, D.R., Head, J.W., 2007. Antarctic dry valleys: microclimate zonation, variable geomorphic processes, and implications for assessing climate change on Mars. Icarus 192, 187–222.
McEwen, A.S., Eliason, E.M., Bergstrom, J.W., Bridges, N.T., Hansen, C.J., Delamere, W.A., Grant, J.A., Gulick, V.C., Herkenhoff, K.E., Keszthelyi, L., Kirk, R.L., Mellon, M.T., Squyres, S.W., Thomas, N., Weitz, C.M., 2007. Mars Reconnaissance Orbiter's High Resolution Imaging Science Experiment (HiRISE). J. Geophys. Res. 112 (E05S02). doi:10.1029/2005JE002605.
Morgenstern, A., Hauber, E., Reiss, D., van Gasselt, S., Grosse, G., 2007. Deposition and degradation of a volatile-rich layer in Utopia Planitia and implications for climate history on Mars. J. Geophys. Res.: Planets 112 (E6). doi:10.1029/2006JE002869.
Moscardelli, L., Doolet, T., Dunlap, D., Jackson, M., Wood, L., 2012. Deep-water polygonal fault systems as terrestrial analogs for large-scale Martian polygonal terrains. GSA Today 22 (8), 4–9.
Neal, J.T., Langer, A.M., Kerr, P.F., 1968. Giant desiccation polygons of Great Basin playas. Geol. Soc. Am. Bull. 79, 69–90.
Orloff, T.C., Kreslavsky, M.A., Asphaug, E.I., 2013. Possible mechanism of boulder clustering on Mars. Icarus 225 (2), 992–999.
Pechmann, J.C., 1980. The origin of polygonal troughs on the Northern Plains of Mars. Icarus 42 (2), 185–210.
Peck, D.L., Minakami, T., 1968. The formation of columnar joints in the upper part of Kilauean Lava Lakes, Hawaii. Geol. Soc. Am. Bull. 79, 1151–1166.
Pewe, T.L., 1959. Sand wedge polygons (tesselations) in the McMurdo Sound Region, Antarctica. Am. J. Sci. 257, 545–552.
Plug, L.J., Werner, B.T., 2001. Fracture networks in frozen ground. J. Geophys. Res. 106 (B5), 8599–8613.
Pratt, B.R., 1998. Molar-tooth structure in Proterozoic carbonate rocks: origin from synsedimentary earthquakes, and implications for the nature and evolution of basins and marine sediment. Geol. Soc. Am. Bull. 110 (8), 1028–1045.
R Core Team, 2013. R: A Language and Environment for Statistical Computing. R Foundation for Statistical Computing, Vienna, Austria URL http://www.R-project.org/ .
Rodríguez, J.A.P., Sasaki, S., Dohm, J.M., Tanaka, K.L., Strom, B., Kargel, J., Kuzmin, R., Miyamoto, H., Spray, J.G., Fairén, A.G., Komatsu, G., 2005. Control of impact crater fracture systems on subsurface hydrology, ground subsidence, and collapse, Mars. J. Geophys. Res. 110 (E06003). doi:10.1029/2004JE002365.
RStudio Team, 2015. RStudio: Integrated Development for R. RStudio. Inc., Boston, MA URL http://www.rstudio.com/ .
Seibert, N.Mand, Kargel, J.S., 2001. Small-scale Martian polygonal terrain: implications for liquid surface water. Geophys. Res. Lett. 28 (5), 899–902.
Séjourné, A., Costard, F., Gargani, J., Soare, R.J., Fedoroc, A., Marmo, C., 2011. Scalloped depressions and small-sized polygons in western Utopia Planitia, Mars: a new formation hypothesis. Planet. Space Sci. 59 (5-6), 412–422.
Sletten, R.S., Hallet, B., Fletcher, R.C., 2003. Resurfacing time of terrestrial surfaces by the formation and maturation of polygonal patterned ground. J. Geophys. Res. 108 (E4). doi:10.1029/2002JE001914.
Soare, R.J., Osinski, G.R., Roehm, C.L., 2008. Thermokarst lakes and ponds on Mars in the very recent (late Amazonian) past. Earth Planet. Sci. Lett. 272, 382–393.
Soare, R.J., Conway, S.J., Gallagher, C., Dohm, J.M., 2016. Sorted (clastic) polygons in the Argyre region, Mars, and possible evidence of pre- and post-glacial periglaciation in the Late Amazonian Epoch. Icarus 264, 184–197.
Tewksbury, B.J., Hogan, J.P., Kattenhorn, S.A., Mehrtens, C.J., Tarabees, E.A., 2014. Polygonal faults in chalk: insights from extensive exposures of the Khoman Formation, Western Desert. Egypt. Geol. 42 (6), 479–482.
Toramaru, A., Matsumoto, T., 2004. Columnar joint morphology and cooling rate: a starch-water mixture experiment. J. Geophys. Res. 109 (B02205). doi:10.1029/2003JB002686.
Treml, V., Krizek, M., Engel, Z., 2010. Classification of patterned ground based on morphometry and site characteristics: a case study from the High Sudetes, Central Europe. Permafr. Periglac. Process. 21, 67–77.
Ulrich, M., Hauber, E., Herzschuh, U., Härtel, S., Schirrmeister, L., 2011. Polygon pattern geomorphometry on Svalbard (Norway) and western Utopia Planitia (Mars) using high-resolution stereo remote-sensing data. Geomorphology 134, 197–216.
Washburn, A.L., 1956. Classification of patterned ground and review of suggested origins. Bull. Geolog. Soc. Am. 67, 823–866.
Watterson, J., Walsh, J., Nicol, A., Nell, P.A.R., Bretan, P.G., 2000. Geometry and origin of a polygonal fault system. J. Geolog. Soc., London 157, 151–162.
Weinberger, R., 2001. Evolution of polygonal patterns in stratified mud during desiccation: the role of flaw distribution and layer boundaries. Geol. Soc. Am. Bull. 113 (1), 20–31.
Werner, S.C., 2008. The early Martian evolution - constraints from basin formation ages. Icarus 195, 45–60.
Williams, R., Robinson, D., 1989. Origin and distribution of polygonal cracking of rock surfaces. Geogr. Ann., Ser. A 145–159.
Wilson, P., Sellier, D., 1995. Active patterned ground and cryoturbation on Muckish mountain, Co. Donegal, Ireland. Permafr. Periglac. Process. 6, 15–25.
Yoshikawa, K., 2003. Origin of the polygons and the thickness of the Vastitas Borealis formation in Western Utopia Planitia on Mars. Geophys. Res. Lett. 30 (12). doi:10.1029/2003GL017165.
Xiao, Z., Zeng, Z., Li, Z., Blair, D.M., Xiao, L., 2014. Cooling fractures in impact melt deposits on the Moon and Mercury: implications for cooling solely by thermal radiation. J. Geophys. Res. 119, 1496–1515. doi:10.1002/2013JE004560.
Zuber, M.T., Smith, D.E., Solomon, S.C., Muhleman, D.O., Head, J.W., Garvin, J.B., Abshire, J.B., Bufton, J.L., 1992. The Mars Observer Laser Altimeter investigation. J. Geophys. Res. 97 (E5), 7781–7797.